

Copyright
by
YONG-MOOK KIM
2000

**A STUDY OF PIPE SPLICE SLEEVES
FOR USE IN PRECAST BEAM-COLUMN CONNECTIONS**

by

YONG-MOOK KIM, B.S.C.E

Thesis

Presented to the Faculty of the Graduate School of

The University of Texas at Austin

in Partial Fulfillment

of the Requirements

for the Degree of

MASTER OF SCIENCE IN ENGINEERING

The University of Texas at Austin

December, 2000

**A STUDY OF PIPE SPLICE SLEEVES
FOR USE IN PRECAST BEAM-COLUMN CONNECTIONS**

**Approved by
Supervising Committee:**

To my devoted wife

Acknowledgements

The research program presented in this thesis was carried out at the Phil M. Ferguson Structural Engineering Laboratory at the University of Texas at Austin. This research was a part of the US-PRESS program by support from the National Science Foundation under grant number BCS-9122950.

I would like to sincerely thank my supervisor, professor Michael E, Kreger, for his suggestions and instructions. His support throughout this research is deeply appreciated. I would also like to thank professor for his time in reviewing and commenting on this thesis.

The assistance of the technical and administrative staff of Ferguson Structural Engineering Laboratory is deeply acknowledged. It was a great pleasure working with them.

Finally, I thank my devoted wife for her great support and encouragement.

Yong-mook Kim

Austin, Texas

December, 2000

Abstract

A STUDY OF PIPE SPLICE SLEEVES FOR USE IN PRECAST BEAM-COLUMN CONNECTIONS

Publication No. _____

Yong-Mook Kim, M.S.E.

The University of Texas at Austin, 2000

Supervisor: Michael E. Kreger

One of the primary objectives of this study was to examine the behavior of a grout-filled pipe sleeve developed to splice longitudinal reinforcement in seismic-resistant precast concrete columns. The secondary objective was to identify problems in the implementation of the prototype splice design and develop improved details of splice sleeves. In order to evaluate the seismic performance of grout-filled sleeves, two precast column specimens, which were connected to a rigid concrete base element by two different types of splice sleeves, were constructed and tested. The behavior of the precast column specimens were compared with the response of a comparable cast-in-place

concrete specimen. In particular, comparisons of connection strength, stiffness, ductility, energy absorption, and failure mode are made.

Although response of the well-behaved precast connection and monolithic connection was not identical, test results indicate that the precast connection should provide sufficient strength and toughness when capacity-design techniques are used to proportion members and connections in the vicinity of beam-column connections. The problems with the prototype splice sleeve were identified and considered in the redesign of a splice sleeve. The precast specimen with improved splice sleeves could successfully provide results comparable with the monolithic specimen. Also, the test program found that performance of splice sleeves is heavily influenced by the quality of grout material and grout placement in the splice sleeve. Consequently, under careful control over assembly and grouting procedure, the splice sleeve type tested in this research could offer satisfying performance for precast concrete structures in seismic regions.

Table of Contents

| | |
|--|-----|
| List of Tables | xi |
| List of Figures | xii |
| Chapter 1: INTRODUCTION | 1 |
| 1.1 CONNECTION DESIGN FOR A PRECAST FRAME BUILDINGS.... | 1 |
| 1.2 DEVELOPMENT OF SPLICE SLEEVE | 3 |
| 1.2.1 Development of the prototype splice | 3 |
| 1.2.2 Behavior of confined grout | 5 |
| 1.2.3 Bond strength under repeated and reversed cyclic loading | 7 |
| 1.3 RESEARCH OBJECTIVES | 7 |
| Chapter 2: DESCRIPTION OF EXPERIMENTAL PROGRAM | 8 |
| 2.1 DESIGN OBJECTIVES | 8 |
| 2.2 DESIGNATION OF TEST SPECIMENS | 9 |
| 2.3 DESCRIPTION OF TEST SPECIMENS | 9 |
| 2.3.1 Specimen Design and Reinforcement Details | 11 |
| 2.3.2 Splice Sleeve Design and Details | 19 |
| 2.3.3 Material Properties | 23 |
| 2.3.4 Fabrication and Erection | 25 |
| 2.4 OBSERVATIONS FROM CONSTRUCTION | 30 |
| 2.5 TEST SETUP | 32 |
| 2.6 DISPLACEMENT HISTORY | 34 |
| 2.7 INSTRUMENTATION | 37 |
| 2.8 TEST PROCEDURE AND DATA ACQUISITION | 41 |
| Chapter 3: PRESENTATION OF TEST RESULTS | 43 |
| 3.1 INTRODUCTION | 43 |
| 3.2 COLUMN SHEAR FORCE - DRIFT ANGLE RELATIONSHIPS | 43 |

| | |
|---|----|
| 3.3 OBSERVED CRACKING AND DAMAGE | 48 |
| 3.3.1 Specimen MC1 | 49 |
| 3.3.2 Specimen PC1 | 53 |
| 3.3.3 Specimen PC2 | 55 |
| 3.4 COLUMN ROTATIONS | 59 |
| 3.5 RESULTS OF AN INDIVIDUAL SPLICE SLEEVE TEST | 61 |
| Chapter 4: EVALUATION OF TEST RESULTS | 65 |
| 4.1 INTRODUCTION | 65 |
| 4.2 PROBLEMS WITH PROTOTYPE SPLICE SLEEVE | 65 |
| 4.3 RESPONSE ENVELOPE CURVES | 69 |
| 4.4 HYSTERETIC BEHAVIOR | 71 |
| 4.4.1 Energy Dissipation | 71 |
| 4.4.2 Equivalent Viscous Damping Ratio | 74 |
| 4.5 COMPARISON OF STIFFNESS AND DUCTILITY | 76 |
| 4.5.1 Secant Stiffness and Ductility | 76 |
| 4.5.2 Stiffness Degradation | 78 |
| 4.5.2.1 Equivalent Stiffness | 81 |
| 4.5.2.2 Peak-to-Peak Stiffness | 82 |
| 4.6 COMPARISON OF RESIDUAL DEFORMATIONS | 84 |
| 4.7 INTERNAL BEHAVIOR OF SPECIMENS | 85 |
| 4.7.1 Strain History of a Column Reinforcing Bar in Specimen MC1 | 86 |
| 4.7.2 Strain History of Column Reinforcing Bar and Splice Sleeve in Specimen PC2 | 87 |
| 4.7.3 Load-Strain Curves of Column Reinforcing Bars | 91 |
| Chapter 5: CONCLUSIONS AND RECOMMENDATIONS | 92 |
| 5.1 INTRODUCTION | 92 |
| 5.2 CONCLUSIONS AND RECOMMENDATIONS | 93 |
| 5.3 ADDITIONAL RESEARCH | 94 |

| | |
|----------------|-----|
| Appendix | 96 |
| Glossary | 97 |
| Reference..... | 99 |
| Vita | 101 |

List of Tables

| | | |
|------------|--|----|
| Table 2.1: | Reinforcing Steel Properties | 23 |
| Table 2.2: | Compressive Strengths of Concrete and Grout | 24 |
| Table 3.1: | Ratios of Column Base Rotation to Column Tip Deflection Angle | 60 |
| Table 4.1: | Calculated and Experimental Strength of Specimens MC1 and PC2 | 71 |
| Table 4.2: | Stiffness and Ductility of Column Specimens | 77 |

List of Figures

| | |
|---|----|
| Figure 1.1: Yielding Mechanisms for Moment Frames..... | 2 |
| Figure 1.2: Prototype Splice | 4 |
| Figure 1.3: Flow of Internal Stresses in the Splice | 6 |
| Figure 2.1: External Dimensions for Specimens | 10 |
| Figure 2.2: Reinforcement Details for Specimen MC1 | 13 |
| Figure 2.3: Cross Section Details for Specimen MC1 | 14 |
| Figure 2.4: Schematic of Connection Concept and Connecting Elements | 15 |
| Figure 2.5: Reinforcement Details for Specimen PC1 | 17 |
| Figure 2.6: Reinforcement Details for Specimen PC2 | 18 |
| Figure 2.7: Details of the Splice Sleeve for Specimen PC1 | 20 |
| Figure 2.8: Details of the Splice Sleeve for Specimen PC2 | 21 |
| Figure 2.9: View of Reinforcement and Formwork (Specimen MC1) | 26 |
| Figure 2.10: View of Reinforcement and Formwork (Specimen PC2) | 27 |
| Figure 2.11: Casting Procedures | 28 |
| Figure 2.12: View of Connection (Specimen PC2) | 29 |
| Figure 2.13: View of Test Setup | 32 |
| Figure 2.14: Test Setup Details | 33 |
| Figure 2.15: Deflected Shape of Column | 35 |
| Figure 2.16: Displacement History | 36 |
| Figure 2.17: Linear Potentiometer Locations | 38 |
| Figure 2.18: Strain Gauge Locations for Specimen MC1 | 39 |
| Figure 2.19: Strain Gauge Locations for Specimens PC1 and PC2 | 40 |

| | |
|---|----|
| Figure 2.20: View of Specimen prior to Testing | 41 |
| Figure 3.1: Shear Force versus Drift Angle for Specimen MC1 | 44 |
| Figure 3.2: Shear Force versus Drift Angle for Specimen PC1 | 45 |
| Figure 3.3: Shear Force versus Drift Angle for Specimen PC2 | 46 |
| Figure 3.4: Crack Patterns for Specimen MC1 | 50 |
| Figure 3.5: Specimen MC1 at Failure..... | 51 |
| Figure 3.6: Failure of Specimen PC1 | 54 |
| Figure 3.7: Crack Opening at the Top of Splice Sleeves (Specimen PC1) | 55 |
| Figure 3.8: Crack Pattern and Damage in Specimen PC2 | 57 |
| Figure 3.9: Photograph of Interface Crack (Specimen PC2)..... | 58 |
| Figure 3.10: Test Setup for Single Splice Sleeve Test | 62 |
| Figure 3.11: View of Spliced Bar after Testing | 63 |
| Figure 3.12: Load-Displacement Plot from Single Splice Sleeve Test | 64 |
| Figure 4.1: Comparison of the Splice Sleeves for Specimens PC1 and PC2 | 66 |
| Figure 4.2: Response Envelopes | 69 |
| Figure 4.3: Cumulative Energy Dissipated | 72 |
| Figure 4.4: Energy Dissipated in the First Cycle of Each Drift Ratio | 73 |
| Figure 4.5: Definition of Equivalent Viscous Damping Ratio, H_{eq} | 74 |
| Figure 4.6: Equivalent Viscous Damping Ratio | 75 |
| Figure 4.7: Definition of Secant Stiffness and Yield Displacement | 77 |
| Figure 4.8: Definition of Stiffnesses | 80 |
| Figure 4.9: Equivalent Stiffness | 81 |
| Figure 4.10: Peak-to-peak Stiffness | 83 |

| | |
|---|----|
| Figure 4.11: Comparison between Equivalent and Peak-to-Peak Stiffnesses | 83 |
| Figure 4.12: Residual Drift Ratios | 84 |
| Figure 4.13: Strain History of Column Reinforcing Bar in Specimen MC1 | 86 |
| Figure 4.14: Strain History of Column Reinforcing Bar in Specimen PC2 | 87 |
| Figure 4.15: Strain History of Splice Sleeve | 88 |
| Figure 4.16: Load-Strain Plot of Column Reinforcing Bar in Specimen MC1 ... | 90 |
| Figure 4.17: Load-Strain Plot of Column Reinforcing Bar in Specimen PC2 | 93 |

CHAPTER 1

INTRODUCTION

1.1 CONNECTION DESIGN FOR PRECAST FRAME BUILDINGS

Precast concrete has proven to be an economical form of construction. Much of the economy of precast framing results from the use of simply-supported single-span beam and deck members. In seismic regions, however, continuity of structural elements is desirable and necessary for at least part of the structural system. Connections between elements should be capable of withstanding many cycles of load reversals while exhibiting ductile behavior. Current design provisions in the Uniform Building Code [1] suggest that connections be able to withstand deformations corresponding with frame drift ratios exceeding 2 percent or more. Because it is advantageous to locate precast connections near the ends of members where lateral load demands are greatest, the behavior of these connections can have a critical impact on the performance of the overall precast system.

Because the amount of energy dissipated by a laterally-loaded frame generally increases with the number of flexural hinges formed, the most desirable mechanism for seismic resistance is a beam-yielding mechanism (Figure 1.1(a)). A single-story column-yielding mechanism (Figure 1.1(b)) does not dissipate nearly as much energy and is likely to result in collapse [5]. The black dots shown in Figure 1.1 represent the plastic hinge locations.

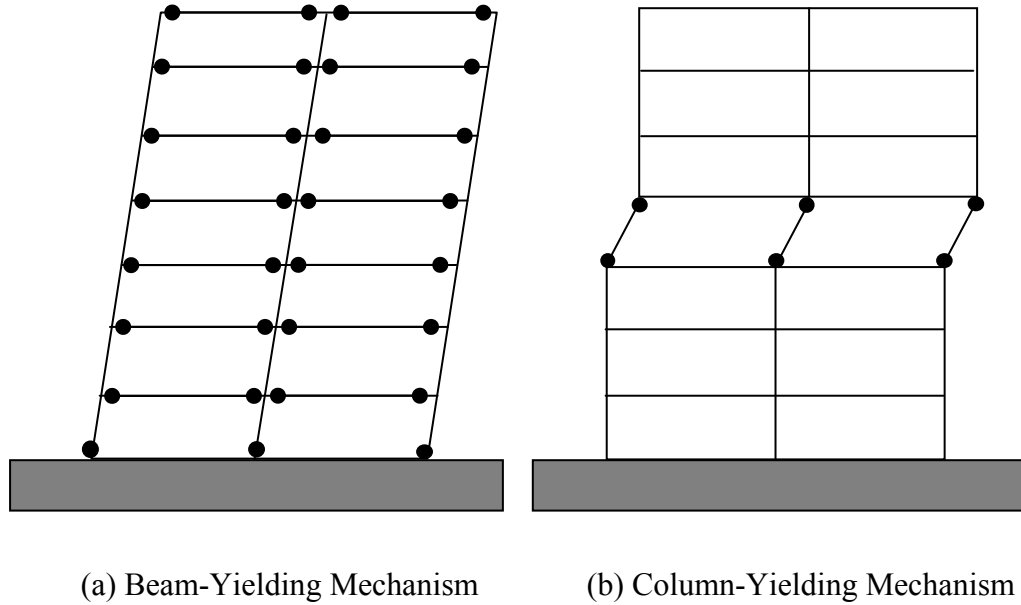


Figure 1.1: Yielding Mechanisms for Moment Frames

Design requirements in the Uniform Building Code [1] are intended to force plastic hinges to form in girder elements of building frames rather than in the columns. The code requires the sum of the flexural strengths of columns at each joint to be at least 20 percent greater than the sum of the flexural strengths of the girders framing into a joint. In other words, the strength of the columns in a ductile moment resisting frame should be some margin greater than the girder strengths. Therefore, the use of the Code provisions requires that we provide the necessary frame ductility through inelastic action in the girder elements, while the columns are intended to remain elastic.

In this study, tests were performed to investigate the behavior of precast column elements connected to a rigid reinforced concrete base. Column

longitudinal reinforcing bars were connected to reinforcement projecting from and anchored in the base element using grout-filled splice sleeves located in the precast column. The assemblage was intended to test a precast column connection that might be used immediately above a floor level. Because the intent of the research was to focus on the behavior of the precast connection, no attempt was made to model the joint and beam(s) at the floor level beneath the connection. Although the connection would not be expected to experience inelastic behavior in an actual structure, connections tested in this study were loaded well into the inelastic response range.

1.2 DEVELOPMENT OF SPLICE SLEEVE

1.2.1 Development of the prototype splice

In precast concrete structures in Asia, mechanical and welded splices in frame elements are commonly used to achieve continuity between precast elements. In the United States, the American Concrete Institute (ACI) Building Code Requirements for Structural Concrete [2] specify that 125% of the nominal yield strength and the specified tensile strength of reinforcement be developed if a mechanical splice is used within two member depths of a column or beam face, or where yielding of reinforcement is likely to occur.

Einea et al. [4] studied four types of grout-filled splice sleeves for precast concrete construction. One of the splice types that were tested by Einea et al. in direct tension was adopted as the prototype splice. The design of splice specimens tested in this study was based on design recommendations from their research.

They investigated the effects of grout compressive strength, wall thickness and diameter of the pipe sleeve, diameter of the spliced bars, and confinement action on the bond strength of spliced bars. Figure 1.2 shows the prototype splice used in the study described herein.

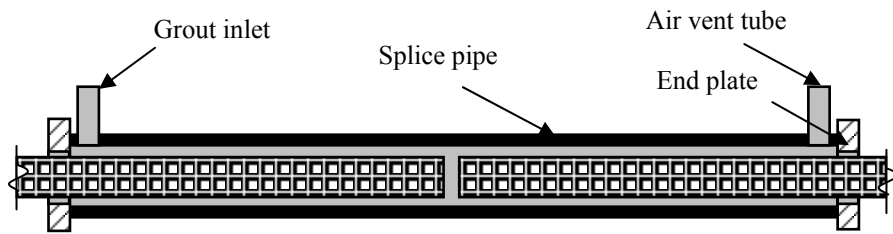


Figure 1.2: Prototype Splice

Using the following relationship for average bond stress, U , at failure,

$$U = \frac{P}{\pi D L_d}$$

where

P = failure load

D = nominal diameter of the bar

L_d = embedment length of a spliced bar,

Einea et al. suggested that

$$U = k \sqrt{f'_{cg}}$$

where f'_{cg} is the specified compressive strength of the grout, and k is a constant value taken to be 38 for the splice type used in this study.

Using the above relationships, the embedment length, L_d , for a Grade 60 #8 bar was calculated. To be consistent with the ACI Code requirement for Type 2 mechanical splices, the yield strength used to determine the required embedment length was assumed to be 75 ksi, and grout strength was assumed to be 6 ksi. The resulting embedment length was calculated to be approximately 8 inches, which resulted in a minimum splice length of approximately 16 inches.

1.2.2 Behavior of confined grout

The grout inside the splice sleeve can act as a quasi-brittle, plastic-softening, or plastic-hardening material [8] depending on the level of confinement. Under a high confining stress, very high grout strength can be achieved with plastic hardening.

In this research, the main objective of confining the grout was to increase the bond strength of bars spliced within the sleeve. The growth and widening of potential splitting cracks around the spliced bars can be restrained if the surrounding grout is effectively confined. With longitudinal and circumferential confinement of the grout, increased bond strength and ductile behavior are possible for the splice connection. The ultimate failure mode of the splice sleeve was expected to be a pullout failure of the bars in the splice sleeve at a load well beyond yield of the reinforcing bars. Figure 1.3 illustrates the expected flow of stresses in the splice sleeve, grout, reinforcement, and concrete.

Soroushian et al. [8] investigated the local bond stress behavior of deformed bars in confined concrete. They found that ultimate bond strength is directly proportional to the square root of the compressive strength of the

concrete. This is consistent with the average bond stress formula developed in the research conducted by Einea et al. [4].

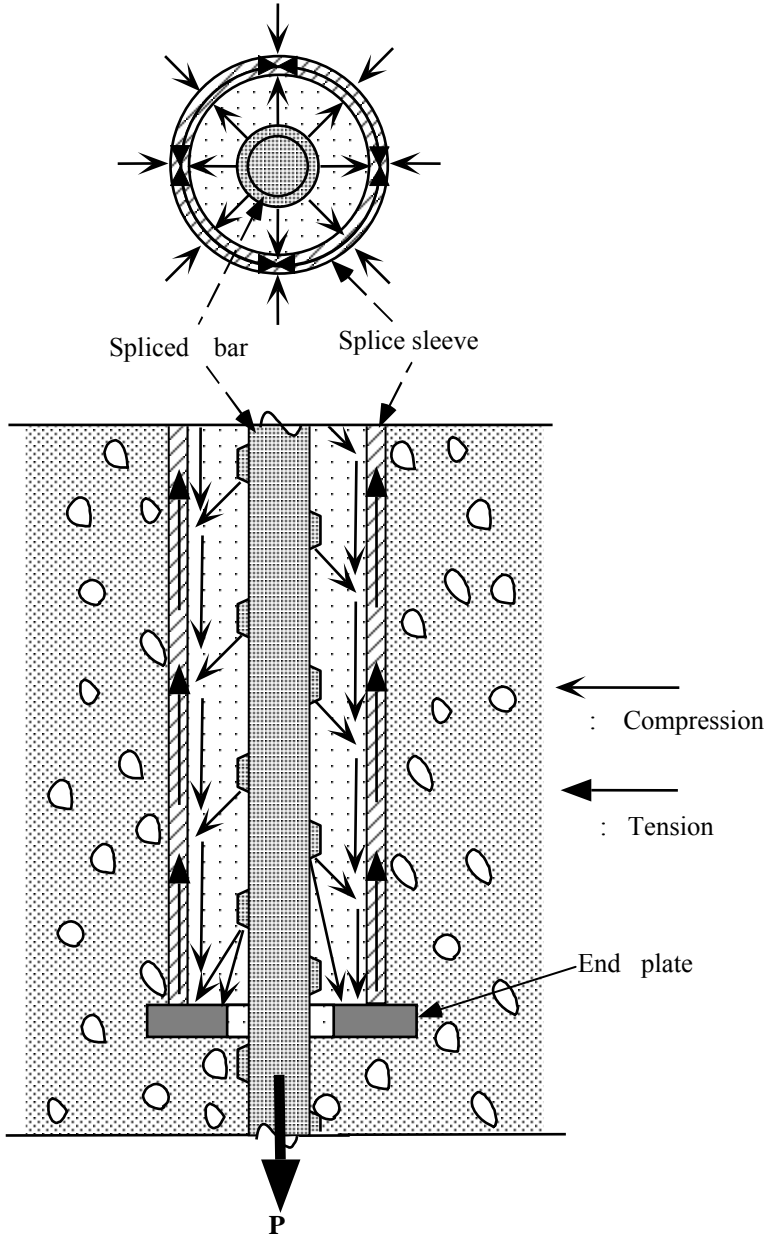


Figure 1.3: Flow of Internal Stresses in the Splice

1.2.3 Bond strength under repeated and reversed cyclic loading

In a seismic region, longitudinal bars in a structure can experience severe reversed cyclic loading during an earthquake. As the tensile force in a bar increases, some slip takes place in the vicinity of flexural cracks that would likely be located at the ends of splice sleeves if bars were spliced at member ends. Slip of bars in the ends of splice sleeves will likely result in bar lugs bearing against the grout. As local crushing occurs in the grout, bars will slip further bringing more lugs into bearing against the grout. The combination of inelastic response of the bars coupled with local crushing of grout will result in residual deformations in splices. When load is reversed, slip will likely occur before the bars can resist significant compression forces. As the number of loading cycles increase, the residual slip will also likely increase, resulting in reduced connection stiffness [6].

1.3 RESEARCH OBJECTIVES

The main objective of this research was to study the viability of grout-filled sleeves to connect longitudinal reinforcement in precast concrete members used in seismic regions. In order to evaluate the seismic performance, results of tests on precast column specimens connected to a rigid concrete base element are compared with the response of a comparable cast-in-place concrete specimen. In particular, comparisons of connection strength, stiffness, ductility, energy absorption, and failure mode are made.

The secondary objective was to identify problems in the implementation of the prototype splice design and develop improved details that were tested in a later specimen.

CHAPTER 2

DESCRIPTION OF EXPERIMENTAL PROGRAM

2.1 DESIGN OBJECTIVES

Three specimens, two simulating a precast beam-column connection and one monolithic connection, were tested using reversed cyclic loads. The two specimens incorporating the precast connection were designed using essentially the same design philosophy as for the monolithic specimen, except different details were used in the connection area between base and column elements. All three specimens were designed to investigate non-linear behavior in the column immediately above the base element to which each column was connected. This was done to examine the limitations of a precast connection in such a location, not because yielding is generally desired at that location; modern design codes require column flexural capacity at a beam-column connection to be significantly larger than beam flexural strength to promote non-linear behavior in the beams and not in the columns.

During design of the specimens, everything required for connecting column elements to base elements was embedded in the elements to minimize or eliminate cast-in-place concrete and the need for falsework during erection. This demanded that careful attention be paid to the precise arrangement and location of connection hardware during fabrication of the specimen components. The

connection details used in the precast specimens were developed with the intent that they could be used in actual precast construction.

2.2 DESIGNATION OF TEST SPECIMENS

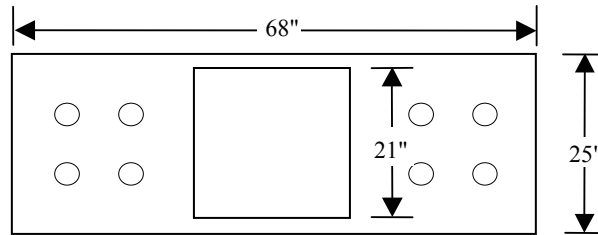
As mentioned previously, three specimens were tested in this study; one with a monolithic connection between the base and column elements, and two with a precast connection. The specimens were designated according to their connection type and order of testing. The monolithic connection was designated MC1, and the precast connection specimens were designated PC1 and PC2.

2.3 DESCRIPTION OF TEST SPECIMENS

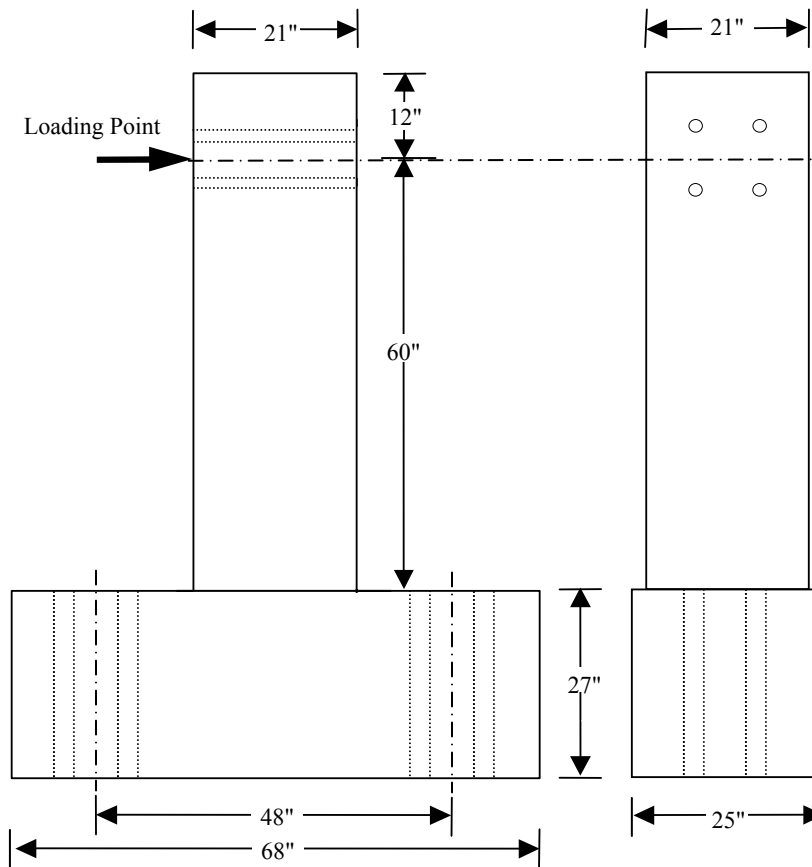
This section presents descriptions, external dimensions, and reinforcement details for each specimen. Material properties and fabrication and erection procedures are also presented.

All specimens had the same external dimensions and were subjected to the same displacement history until failure occurred. Due to the similarity of dimensions and some details, the following discussion applies to all specimens. Details unique to particular specimens are presented in separate sub-sections.

Because this study focused on the performance of the splice connection that would facilitate splicing column longitudinal reinforcement immediately above a continuous precast beam element, test specimens consisted of a half-length column element (effectively from top of beam to column mid-height) and a base element for anchoring column reinforcement and anchoring the specimen to the test floor. Overall dimensions for the specimens are shown in Fig. 2.1.



(a) Top view



(b) Elevation view

(c) Side view

Figure 2.1: External Dimensions for Specimens

Specimen MC1 utilized a monolithic connection between the column and base element. Reinforcement across the interface between the column and base member was continuous. The main purpose of testing this specimen was to collect data for a monolithic connection to compare with data for precast connections.

Specimens PC1 and PC2 utilized grout-filled splice devices to join longitudinal reinforcement in a precast column to a base element. Details of the splice devices used in Specimens PC1 and PC2 will be presented in the following section.

During fabrication, plastic pipes, as shown in Fig. 2.1, were embedded in the base and column element to facilitate connection of each specimen to the testing floor and hydraulic ram used to load each specimen. The base element of each specimen was tied to the test floor with 1-1/2 in. dia. prestressed thread bars. A hydraulic ram was connected to the column tip using four 5/8-in. dia. Dywidag bars.

2.3.1 Specimen Design and Reinforcement Details

In this study, the following conditions were incorporated in the design of the specimens:

- No axial force is imposed on the column.
- The plastic hinge will occur in the column adjacent to the base element.
- The base element is sufficiently stiff and restrained by the floor to prevent any rotation of the base element.

All test specimens were designed with the same reinforcement details except that column longitudinal bars in Specimen MC1 were continuous and were

spliced in Specimens PC1 and PC2. Twelve #8 Grade 60 bars were used as the column longitudinal reinforcement. Four #9 bars were used as the top and bottom longitudinal reinforcement in the base element. All base elements were designed to have at least 20 percent more flexural strength than the column elements. The reinforcement requirements were calculated for each base element by assuming it to be a simple pin-supported beam. Because the base element was tied down to the test floor, actual strength demands were far less than those based on the assumptions just noted.

Reinforcement details for Specimen MC1 and selected cross sections are shown in Figs. 2.2 and 2.3. The column longitudinal reinforcement used in this study was anchored at the top of the column and in the base element using 90-degree hooks, which resulted in significant congestion. Because the longitudinal bars were continuous in Specimen MC1, fabrication of the steel cage was much more difficult than for the precast specimens. Design of shear reinforcement for both the column and base element was carried out according to Chapter 21 of the ACI 318 Building Code [2]. Shear reinforcement details were the same for all specimens. For the base elements and the column sections in the plastic hinge region (which was assumed to range from the member interface to a height approximately 20 in. above the base), design for shear resulted in 4 in. spacing of two sets of #4 rectangular hoops. The same hoops with 6-in. spacing were used for the remainder of the column height. In the plastic hinge region, two #4 cross-ties were added to each set of hoops to provide additional concrete confinement.

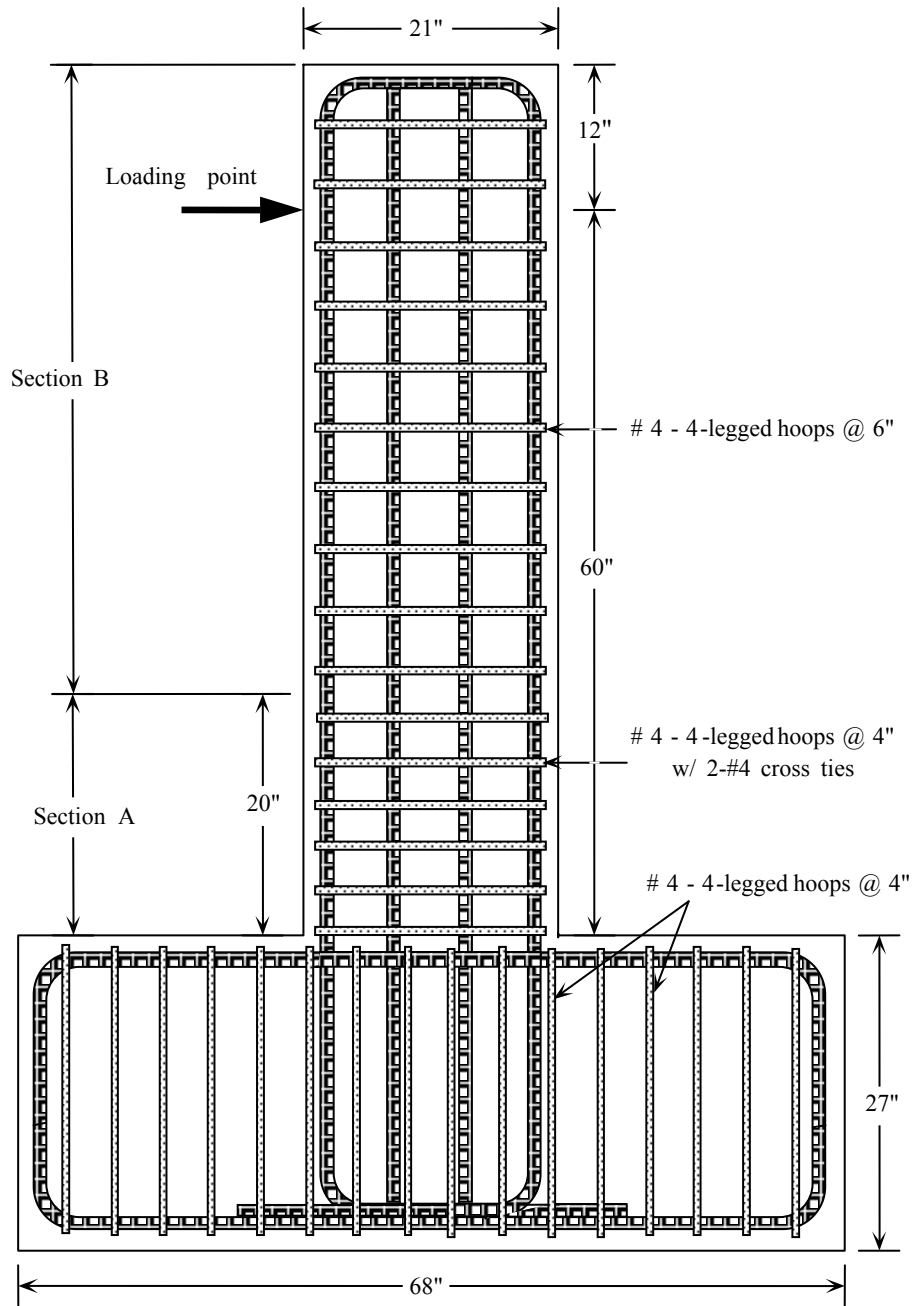
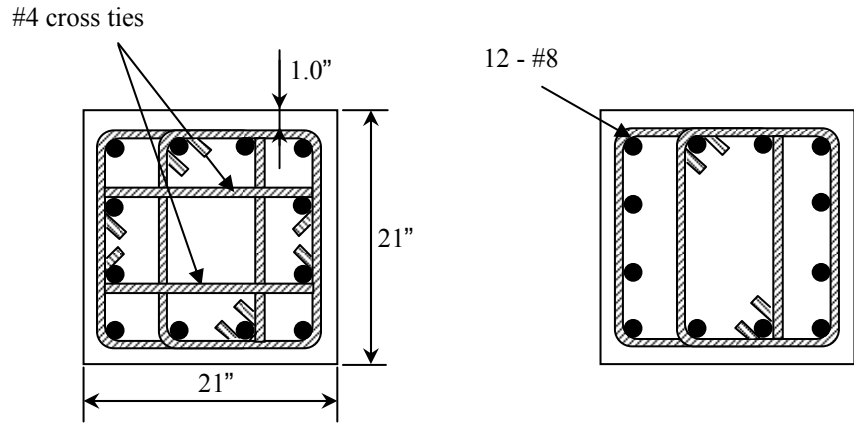
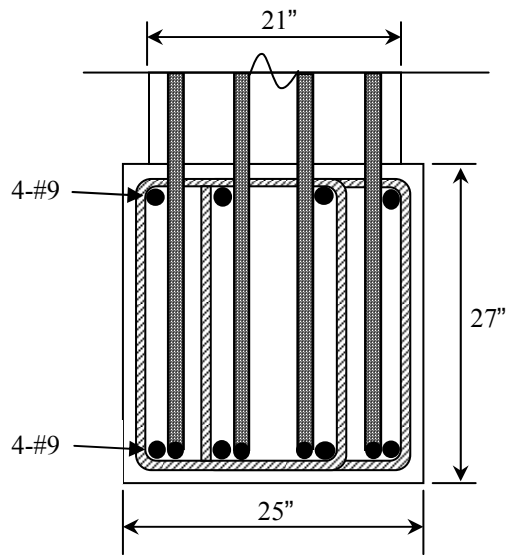


Figure 2.2: Reinforcement Details for Specimen MC1



(a) Column cross section A

(b) Column cross section B



(c) Base cross section

Figure 2.3: Cross Section Details for Specimen MC1

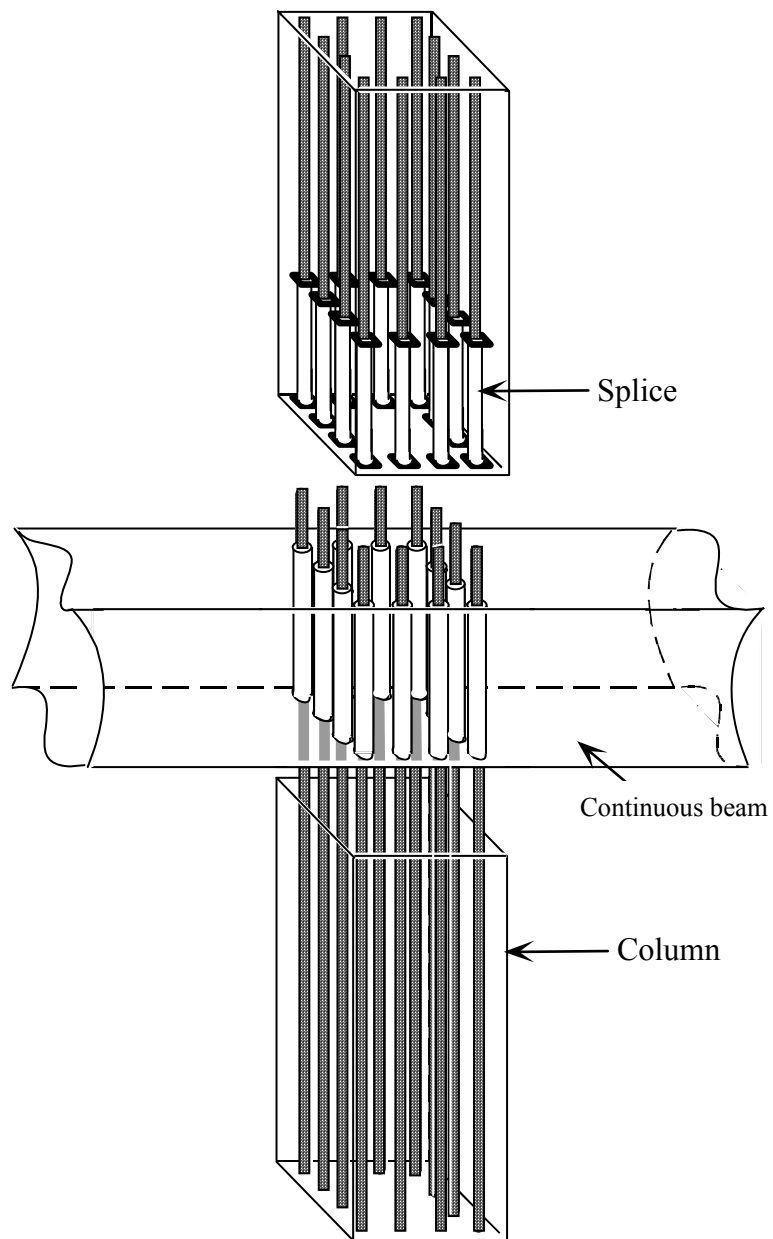


Figure 2.4: Schematic of Connection Concept and Connecting Elements

A precast continuous beam-column connection, like that shown in Fig. 2.4 which incorporates the splice-sleeve connection, would have column longitudinal reinforcement that passes through the beam element. Reinforcement details for the precast specimens, PC1 and PC2, are shown in Figs. 2.5 and 2.6. Details for the splice sleeves used in Specimens PC1 and PC2 are described in the following section. All other reinforcement details were the same as those used in Specimen MC1. The confinement and shear reinforcement details for the plastic hinge region of Specimens PC1 and PC2 are shown in Fig. 2.5. During the fabrication and casting of precast specimens, congestion caused by the longitudinal reinforcement, splice sleeves, and transverse reinforcement in the plastic hinge region required substantial attention.

Concrete cover for the column longitudinal reinforcing bars in all specimens was designed with 1-1/2 in. thickness. According to Chapter 7 of the ACI 318 Building Code, the minimum concrete cover for primary reinforcement in precast concrete is specified as d_b , which would result in 1.0 in. concrete cover for #8 bars in the test specimens. Specimens PC1 and PC2, however, contained 2.0 in. and 2-1/4 in. outside-diameter splice sleeves respectively. Therefore, both specimens required at least 1-1/2 in. concrete cover for longitudinal reinforcing bars because those bars were centered with the splice sleeves. In order to have the same reinforcement details, the same concrete cover was used for all specimens. Concrete cover for primary reinforcement in all base elements was 1-1/8 inches.

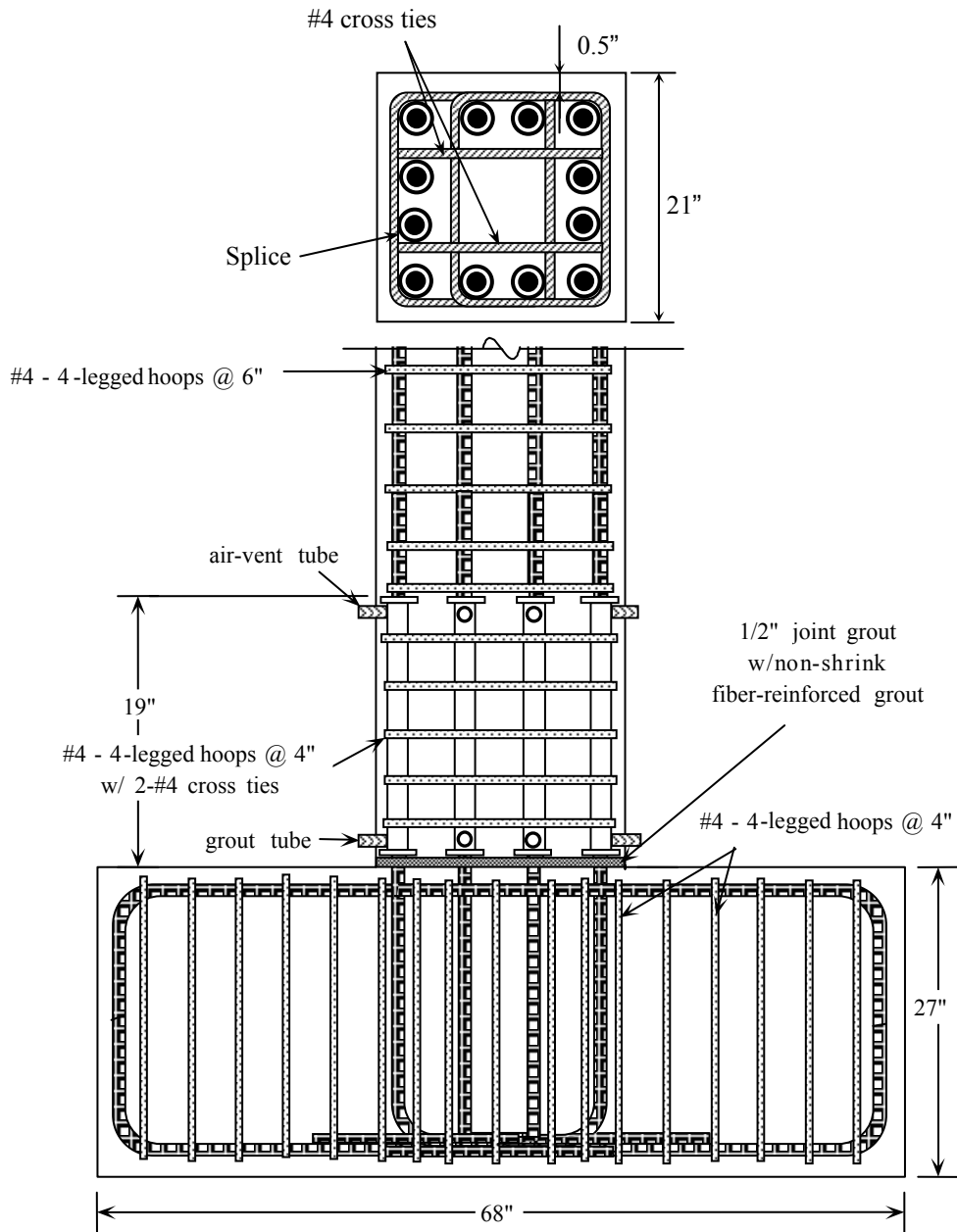


Figure 2.5: Reinforcement Details for Specimen PC1

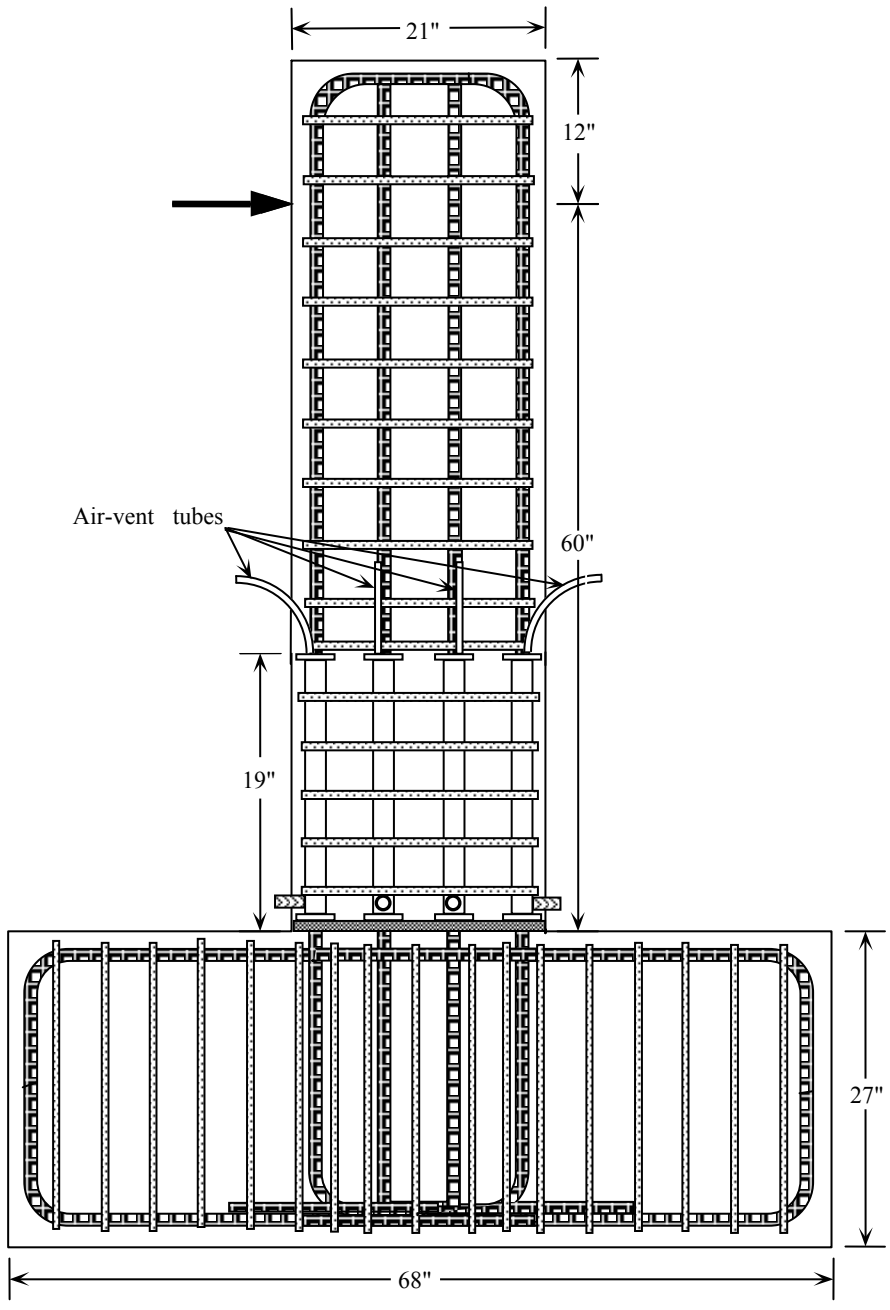


Figure 2.6: Reinforcement Details for Specimen PC2

2.3.2 Splice Sleeve Design and Details

The prototype splice design was based on the study by Einea et al. [4]. According to their research, the required embedment length for a Grade 60 #8 bar for the splice type used was approximately 8 in., resulting in a required total splice length of 16 inches. Considering that some gap between the ends of the spliced bars will be necessary to accommodate fit, a final splice sleeve length of 17 in. was used. Details of the splice sleeve used in Specimen PC1 are shown in Fig. 2.7.

Splice sleeves for Specimen PC1 consisted of a 17-in. long commercially available steel pipe and two 2.5 x 2.5 x 3/8 in. steel plates. The pipe used to fabricate the splice sleeve for Specimen PC1 was ASTM A53 TYPE S Grade B pipe with a minimum yield stress of 35 ksi and a minimum tensile strength of 60 ksi. Dimensions of the pipe section, as shown in Figure 2.7, were 2.0 in. outside diameter and 1.5-in. inside diameter. Holes in the end plates were 1.25-in. diameter, which was 0.25 in. larger than the nominal diameter of the spliced bars. The end plates were welded in the laboratory to the pipe sleeve.

The splice sleeve for Specimen PC1 had top and bottom grout holes drilled at both ends of the pipe. The diameter of the holes was 0.5 in. The grout holes were located approximately 3/8 in. away from the end of the pipe to avoid the weld metal between the pipe and the end plates. The location of the top grout outlet resulted in major problems for this splice sleeve. The problems will be discussed in Chapter 4.

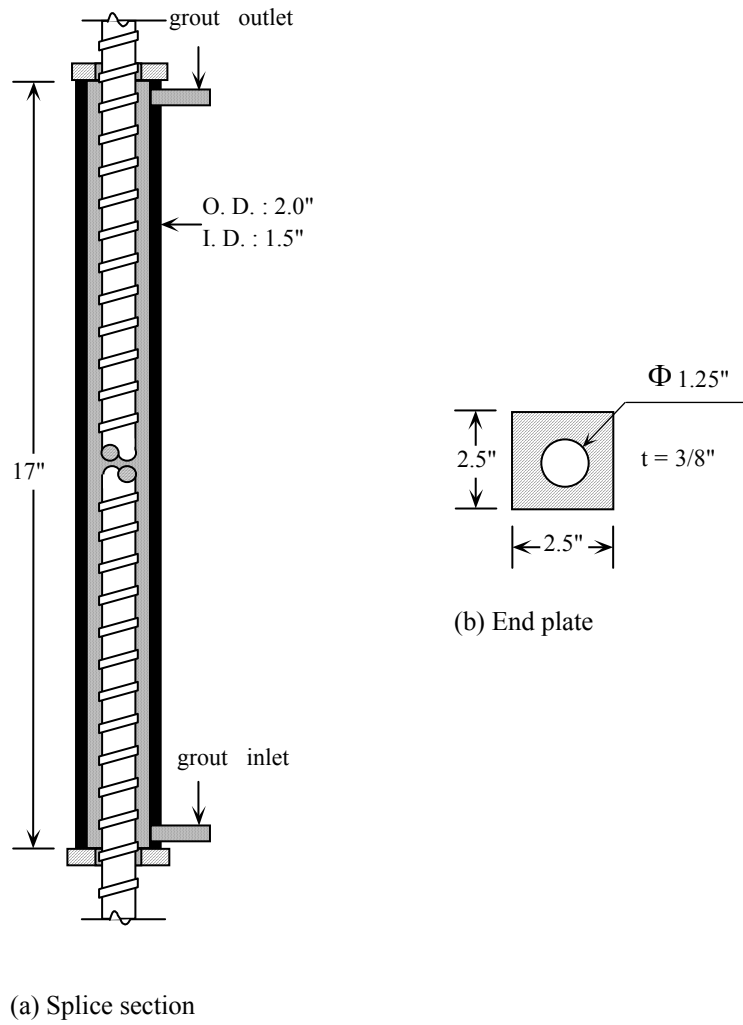


Figure 2.7: Details of the Splice Sleeve for Specimen PC1

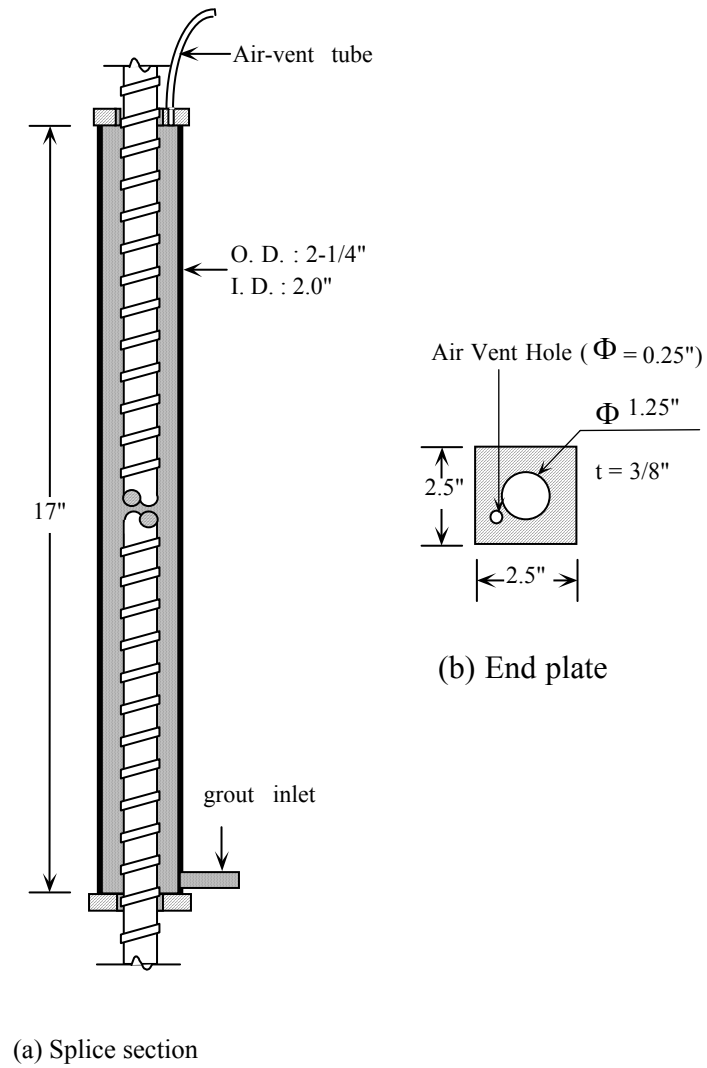


Figure 2.8: Details of the Splice Sleeve for Specimen PC2

The splice sleeves were revised after testing Specimen PC1. The first change was to increase the inside diameter of the pipe to facilitate injection of grout. The dimensions of the pipe section, as shown in Figure 2.8, were 2-1/4 in. outside diameter and 2.0 in. inside diameter. The increase of inside diameter, however, resulted in a loss of cross section area. Therefore, the material strength of the pipe had to be increased. As a result, a seamless DOM (Die-cast On Mandrel) structural tube with minimum yield stress 65 ksi and minimum tensile strength of 80 ksi was used. These values were obtained from the manufacturer's catalog.

Another important adjustment was the change of a grout port location. The bottom grout port where grout was injected remained in the same location but the grout vent was moved from the top of the pipe to the top end plate (Figure 2.8 (b)). It was also drilled with a smaller diameter because of the limited space between the inside wall of the pipe and the edge of the hole for receiving the reinforcing bar.

When commercially available pre-mixed cement and sand grout (Euclid non-shrink grout) was used in Specimen PC1, great difficulty was experienced while attempting to inject the grout. Consequently, the grout formulation was also changed for Specimen PC2. Instead of cement and sand grout, cement grout containing no sand was used for Specimen PC2. In addition, an expansive admixture was added to the cement grout in Specimen PC2. The mix proportion of expansive admixture was in accordance with a TxDOT (Texas Department of Transportation) standard, which recommends approximately 1% of expansive

agent by weight. SIKA's Interplast-N was used as the expansive admixture and was added at a rate of 0.9% of the Type I cement weight. The main purpose of using the expansive admixture was to compensate for the volume decrease due to drying shrinkage. This expansive force can also result in a prestressing effect if confined properly. The increase of confining pressure from the grout expansion was not explicitly considered in this study. After several sample cube tests, and considering required strength and workability, a water/cement ratio of 0.3 was chosen.

2.3.3 Material Properties

All conventional reinforcing bars used in the specimens were ASTM A615 Grade 60 steel. There were three different kinds of reinforcement used, #4's for shear and confining reinforcement, #8's as the longitudinal column reinforcing bars, and #9's for longitudinal reinforcement in the base elements. Tensile properties of the reinforcement are summarized in Table 2.1. All reinforcement strengths were based on the numerical average of three sample tests.

Table 2.1: Reinforcing Steel Properties

| Bar Size | f_y (ksi) | f_u (ksi) |
|----------|-------------|-------------|
| #4 | 68.5 | 105.2 |
| #8 | 66.3 | 101.3 |
| #9 | 65.5 | 103.1 |

The same nominal concrete design strength was used for all specimens. The design compressive strength of the normal weight concrete was 4000 psi and a maximum coarse aggregate size of 3/8 in. was used. In order to increase the workability and slump, superplasticizer was added in the laboratory to the ready-mixed concrete.

Table 2.2: Compressive Strengths of Concrete and Grout

| Concrete & Grout | | Days | |
|------------------------------------|-----|-----------------------|--|
| | | 28-day strength (psi) | Strength at the first day of testing (psi) |
| Concrete for Specimens | MC1 | 4040 | 4230 |
| | PC1 | 4040 | 4360 |
| | PC2 | 4530 | 4710 |
| Grout for Column-to-base Interface | PC1 | 5710 | Not available |
| | PC2 | 6650 | Not available |
| Grout for Splice sleeves | PC1 | 6640 | 6820 |
| | PC2 | 6040 | 6340 |

Grout used for the interface between the column and base element was normal cement mortar with nylon fibers. Fibers reduced the slump of the material and provided a tough filler material for the gap between the column and the base element that was provided for construction tolerances. Mix ratio for fibers was 0.1

% of grout by weight. Superplasticizer was also added to the grout for splice sleeves in both Specimens PC1 and PC2.

The test specimens and concrete cylinders were cured in the laboratory under plastic sheets for 7 days. After the plastic was removed, they were left open to the air until they were tested. Forms were removed 10 days after casting to reduce possible shrinkage cracks during curing. The strength of concrete, grout in the interface, and grout in the splice sleeve were tested at 28 days, and the concrete and splice sleeve grout were tested on the first day of testing. These strengths are summarized in Table 2.2. The strengths of concrete cylinders and grout cubes were the numerical average of five tests.

Specimens MC1 and PC1 were fabricated and cast together, so they were made from the same concrete mix. The superplasticizer added to the mix for Specimens MC1 and PC1 turned out to be excessive resulting in a slump of more than 10 in., but, as shown in Table 2.2, did not significantly affect the concrete strength. The slump for the Specimen PC2 concrete mix was approximately 6 in.

2.3.4 Fabrication and Erection

Figures 2.9 and 2.10 show the reinforcement cages and formwork for Specimens MC1 and PC2 prior to casting. Specimens were fabricated and cast at the laboratory. All strain gauges on reinforcing bars were attached after the cages were assembled. Wooden forms were coated with form oil prior to setting the reinforcing cages in the forms. Ready-mixed normal-weight concrete was used for all specimens. Consolidation of concrete was achieved using pencil vibrators. Figure 2.11 shows the casting procedure. In the erection process for Specimen

MC1, the entire specimen was moved to the test floor by the crane. Then, through the embedded plastic pipes in the base element, the specimen was tied down to the test floor using 1-1/2 in. diameter threaded bars that were prestressed with sufficient force to resist column yielding. Connecting the ram to the top of the column using 3/8-in. diameter Dywidag bars completed the erection process.

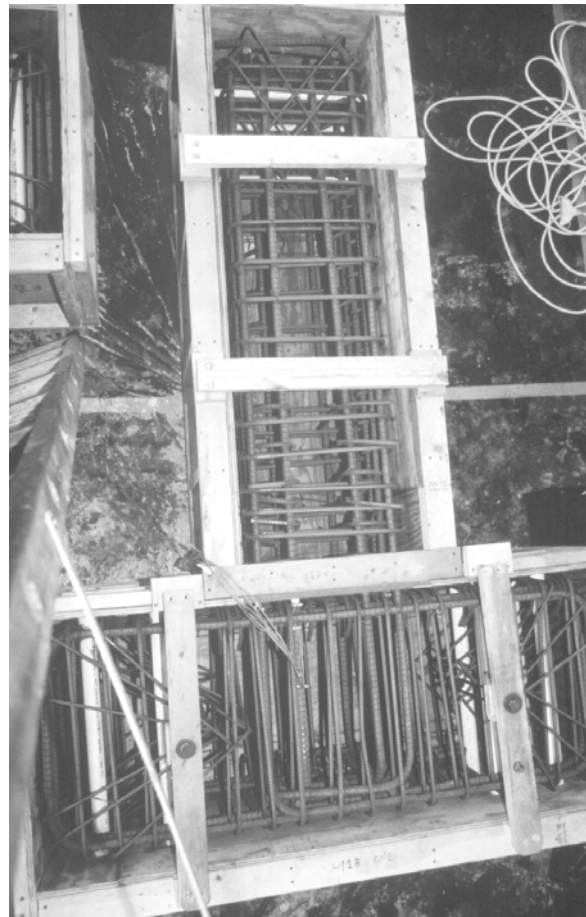
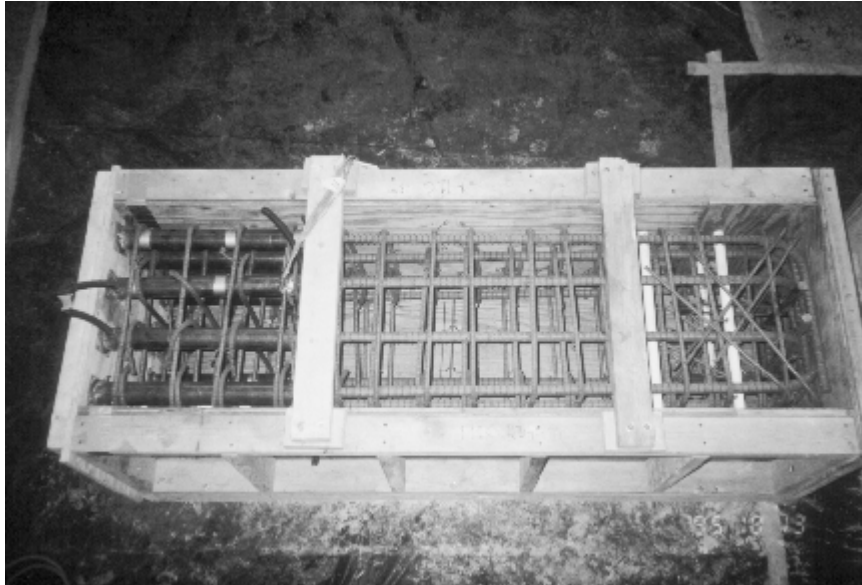
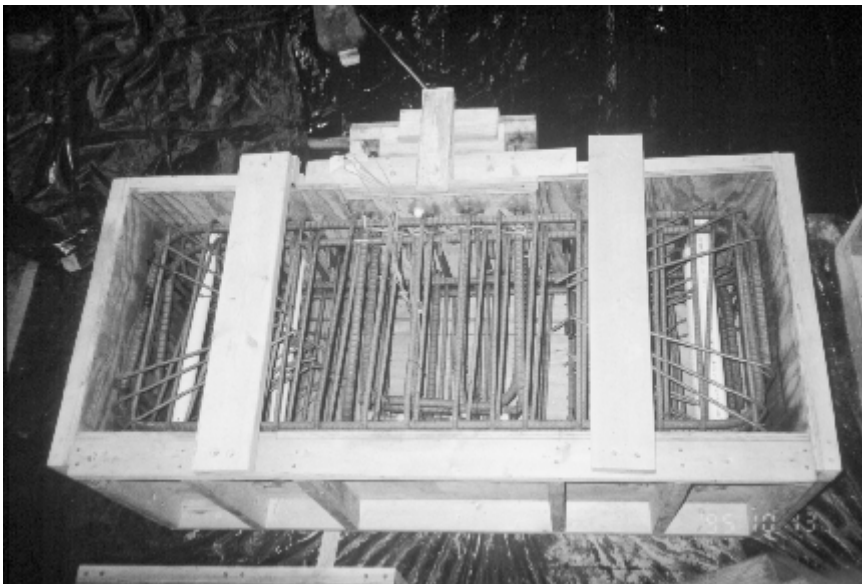


Figure 2.9: View of Reinforcement and Formwork (Specimen MC1)



(a) Column reinforcement cage and formwork



(b) Base reinforcement cage and formwork

Figure 2.10: View of Reinforcement and Formwork (Specimen PC2)

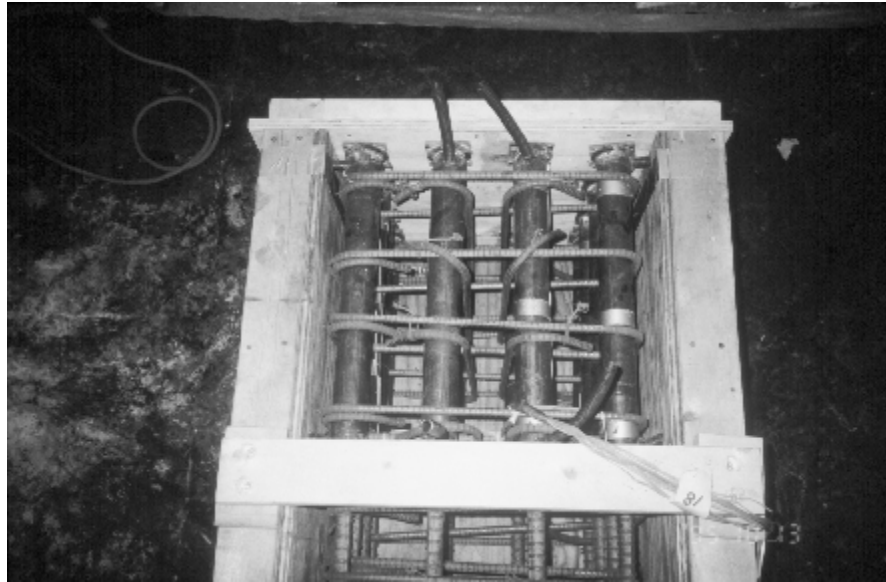


(a) Vibration of concrete

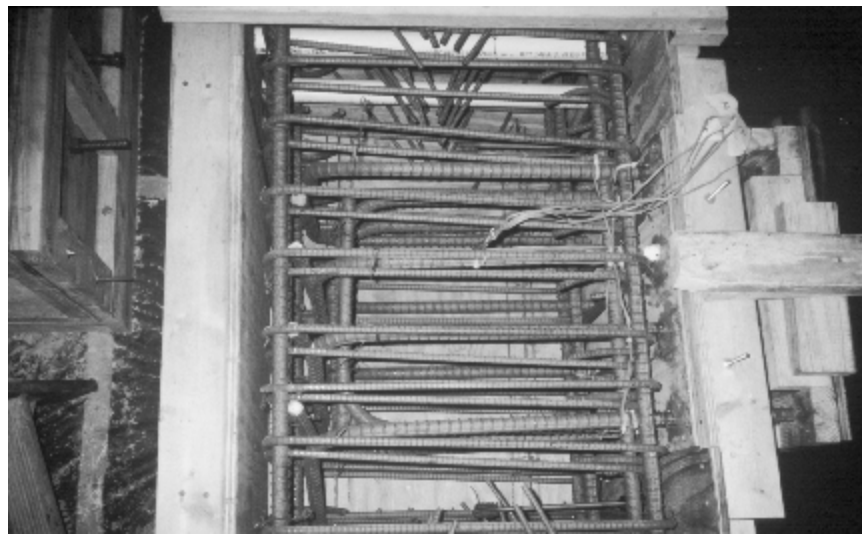


(b) Casting of concrete

Figure 2.11: Casting Procedures



(a) Detail of precast column end



(b) Detail of splice bars in the base element

Figure 2.12: View of Connection (Specimen PC2)

Special consideration was given to the fabrication of forms for Specimens PC1 and PC2. Due to the tight clearance between the holes in the splice sleeves and the spliced reinforcing bars, special care was taken to ensure the alignment of the column reinforcement in the base element. For the alignment of the splice bars extending from the base element, two identical wooden forms with holes at the locations of the reinforcing bars were used to fix those bars in their desired positions (Figure 2.12).

Even though the fabrication of reinforcing cages for Specimens PC1 and PC2 was much easier than for Specimen MC1 because of the discontinuity of column longitudinal reinforcing bars, the added splice sleeves resulted in much more congestion at the base of the column which required special care during concrete casting.

2.4 OBSERVATIONS FROM CONSTRUCTION

One of the major considerations in designing precast concrete connections is ease of fabrication and construction. Some hidden problems during design appeared during the construction process. The objective of this section is to report the problems encountered during construction, especially for specimens with precast elements.

The first problem noticed during construction was reinforcement congestion. As shown in Figure 2.13, at the lower end of the column section, the column longitudinal reinforcing bars were mixed with heavy shear reinforcement and confinement steel in the form of closed hoops and cross ties. In addition, the

splice sleeves that had grout tubes attached at both ends were also present in the end region of the column, which made it difficult to assemble the column cage.

The second problem was related to the splice hole size. Holes in end plates of the splice sleeves had very small tolerances to accommodate the longitudinal reinforcement. This could not be avoided because the confinement of the grout was a key to attaining successful splice sleeves. These small tolerances could introduce fit problems when column longitudinal reinforcing bars are spliced. In order to overcome this tolerance problem, extra caution was exercised when aligning the splice sleeves and longitudinal bars during fabrication.

There were also difficulties encountered during grouting of the splice sleeves. The grouting procedure required special attention to eliminate any voids inside the splice sleeves. Inadequate grouting would result in early loss of column stiffness and development of large cracks between the column and base elements and a large flexural crack in the column. This was actually the main reason for the use of the expansive agent that was added to the grout for the splice sleeves in Specimen PC2. For Specimen PC1, grouting was done using a manual pump, which was easier to control than an electric pump. However due to the slow speed of grouting, the rapid hardening characteristics of the grout resulted in wasting substantial amounts of grout and blockage of the grout ports. In addition, the grouting material for Specimen PC1, Euclid non-shrink grout, contained sand that caused segregation of ingredients when it was injected into the small annular space between the spliced bars and the inside wall of the splice sleeve. It resulted in only cement paste existing near the top of the splice sleeve.

The use of expansive grout also required special attention for mix ratios. Grout cube tests performed to determine the optimum amount of expansive agent indicated that the grout strength is very sensitive to the mix proportions. Therefore, caution must be exercised in batching the grout.

2.5 TEST SETUP

Figure 2.13 shows a specimen after assembly was complete. Details of the test setup are also illustrated in Figure 2.14. The primary loading frame, consisting of two wide flange beams, was attached to the strong reaction wall. The hydraulic ram was attached to this loading frame. Rotation of the column tip in the plane of the specimen was allowed by connecting the hydraulic ram with two horizontal pins to the frame and the specimen.



Figure 2.13: View of Test Setup

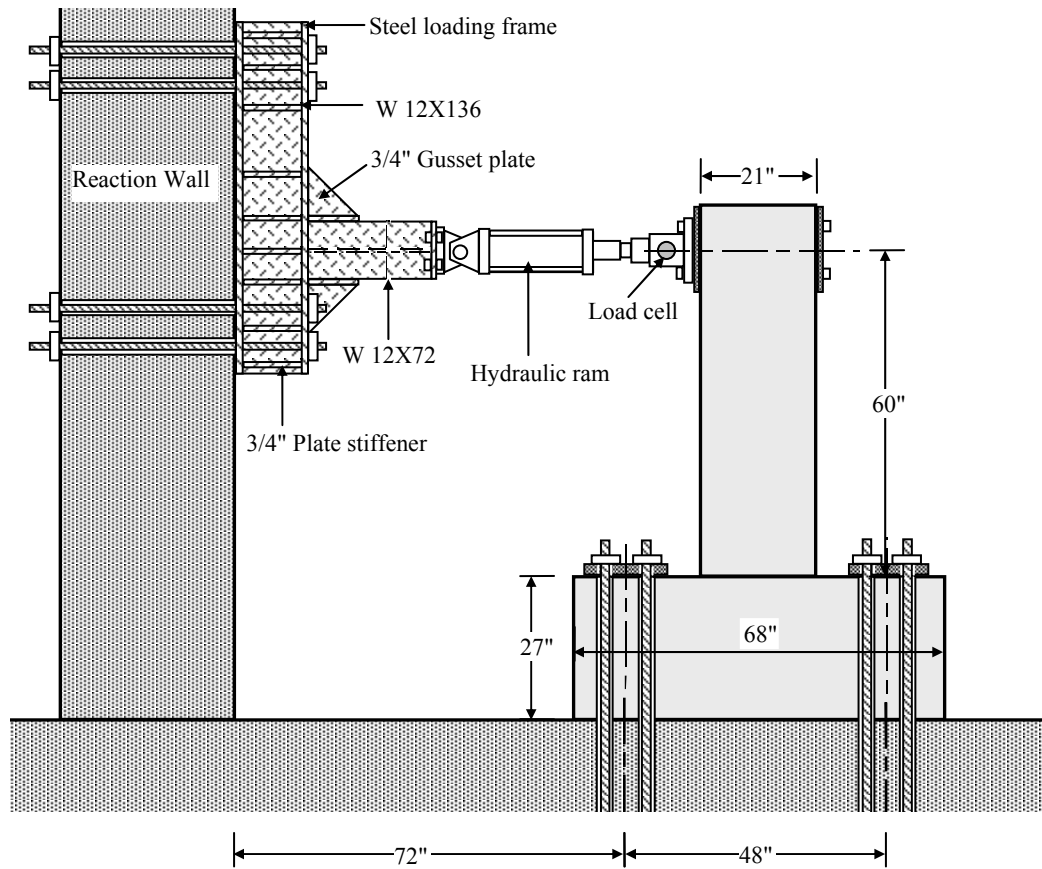


Figure 2.14: Test Setup Details

As shown in Figure 2.14, the loading frame was heavily stiffened with 3/4 in. thick steel plates to avoid local buckling of the frame. Two triangular-shaped gusset plates were used to strengthen the connection between the W shapes supporting the hydraulic ram. The column element of the complete specimen was connected to the ram, and the base element to the floor using the holes provided by the embedded plastic pipes. The base unit was tied to the floor with prestressed 1-1/2 in. dia. threaded bars, and the column was connected to the ram with four 5/8-in. diameter Dywidag bars.

A pin load cell was used to connect the ram to the column. The hydraulic ram used for testing has a capacity of 192 kips in compression and 157 kips in tension. Maximum stroke of the ram is approximately 15 in. Loading of the test specimen was performed using a hydraulic hand pump connected to the ram.

2.6 DISPLACEMENT HISTORY

All specimens were subjected to a reversed cyclic pseudo-static lateral load history in which the controlling parameter was the column end displacement. Lateral load was applied at the column upper end, and no external axial load was applied. The positive sense for load and displacement for the remainder of this report corresponds with loading/displacing away from the strong wall.

Drift is the lateral displacement of a structure or element. Drift angle R is defined as:

$$R = \frac{\Delta}{H}$$

where Δ is the column relative displacement (drift), and H is the column height (Figure 2.15). The displacement history applied to the specimens is shown in Figure 2.16 and is represented using the drift angle R .

Each specimen was subjected to progressively increasing sets of drift reversals. A very small drift ratio such as 0.1 percent was initially applied to check the loading and data acquisition systems at the start of the test. This was followed by a cycle to 0.25 percent drift ratio. Drift ratios were increased by 0.25 percent up to 1.0 percent. The number of cycles for each drift ratio, starting at 0.5 % drift, was three. After reaching 1.0 percent drift ratio, testing progressed with 0.5 percent drift ratio increments until 3.0 percent, then testing continued with 1.0 percent drift ratio increments up to the maximum load.

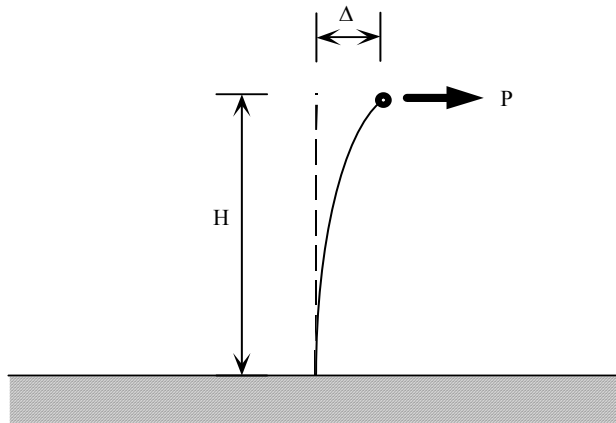


Figure 2.15: Deflected Shape of Column

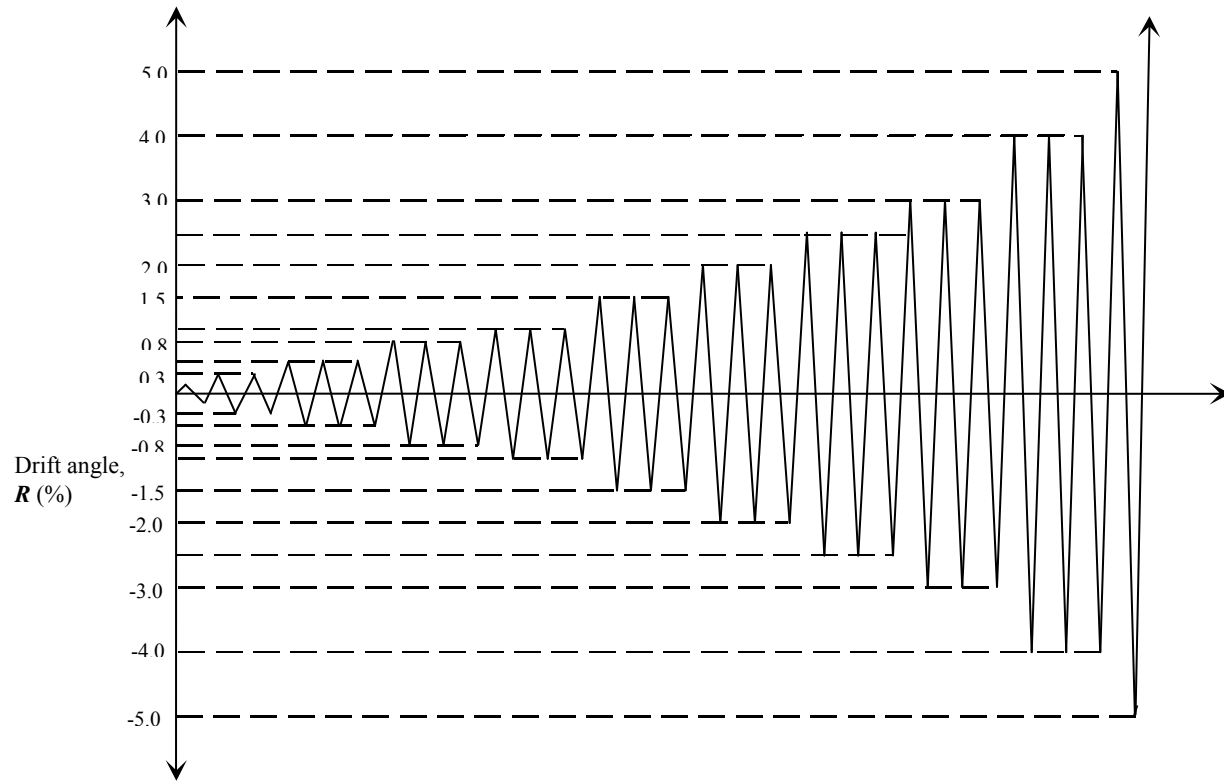


Figure 2.16: Displacement History

In many studies, 2.0 percent drift ratio is often considered to be the maximum deformation that a structure, under earthquake load, should have to withstand [1]. Cycles beyond 2.0 percent drift ratio were considered excessive but made it possible to identify the cause of failure and ductility capacity.

There is one important fact in the calculation of drift ratios for these specimens, which should be mentioned. In a real structure, overall story drift occurs due to the rotation of the column ends in addition to deformations between the column ends. The specimens in this study were restrained to prevent rotation at their base. Therefore, the deformations that were imposed on the columns tend to be quite excessive.

2.7 INSTRUMENTATION

There were three types of instrumentation used: a load cell, linear potentiometers, and strain gauges.

The pin load cell mounted in the hydraulic ram measured the applied lateral load. The capacity of the load cell is 150 kips. In order to measure the lateral column end displacement, a 5-in. string transducer was used. One end of the string transducer was fixed to the loading frame and the other was connected to the mid-depth of the column. Two linear potentiometers on opposite column faces measured column rotations at the base (see Figure 2.17). There were also two additional linear potentiometers mounted on top of the base element to measure sliding of the column base. Selected longitudinal reinforcement in the columns and splice sleeves were instrumented with strain gauges (described below).

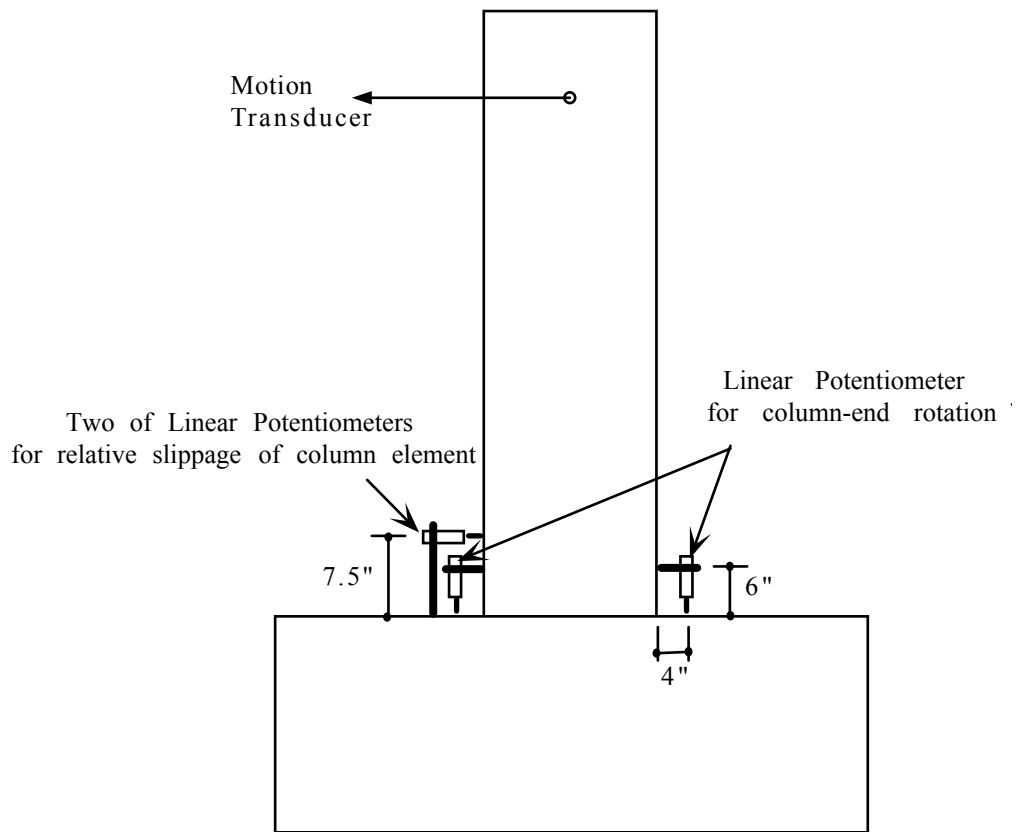


Figure 2.17: Linear Potentiometer Locations

The locations of strain gauges in the specimens are shown in Figures 2.18 and 2.19. For all specimens, six strain gauges were attached on the longitudinal reinforcement at the interface. For Specimens PC1 and PC2, six pairs of strain gauges were attached on six splice sleeves in addition to the strain gauges on the column longitudinal bars. Each set was attached near the bottom end and at the middle of a splice sleeve. A mechanical dial gauge was also used to monitor the column-end deflections during testing.

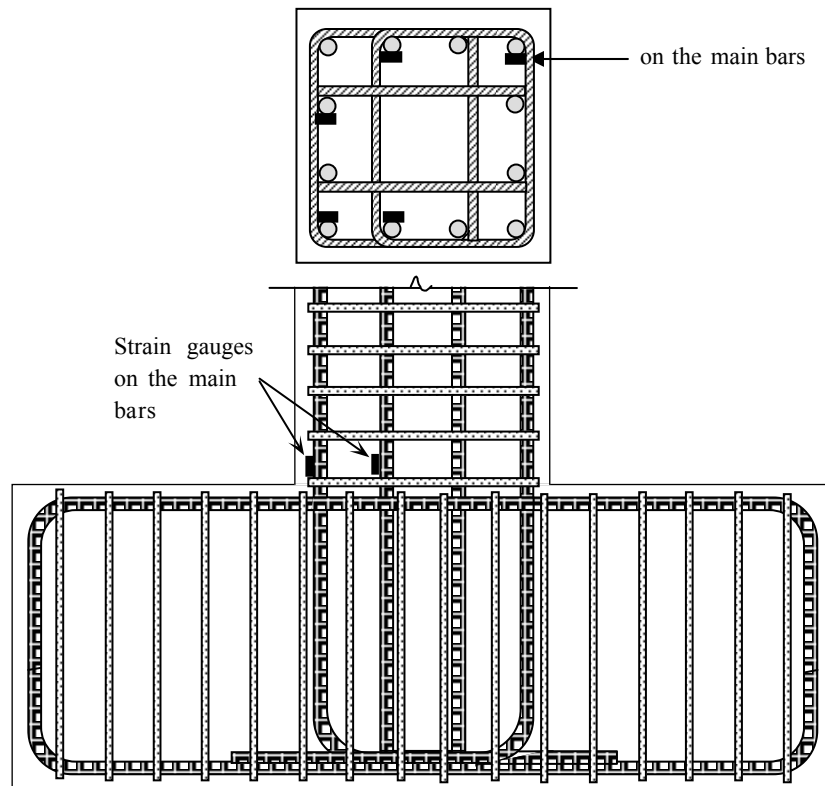


Figure 2.18: Strain Gauge Locations for Specimen MC1

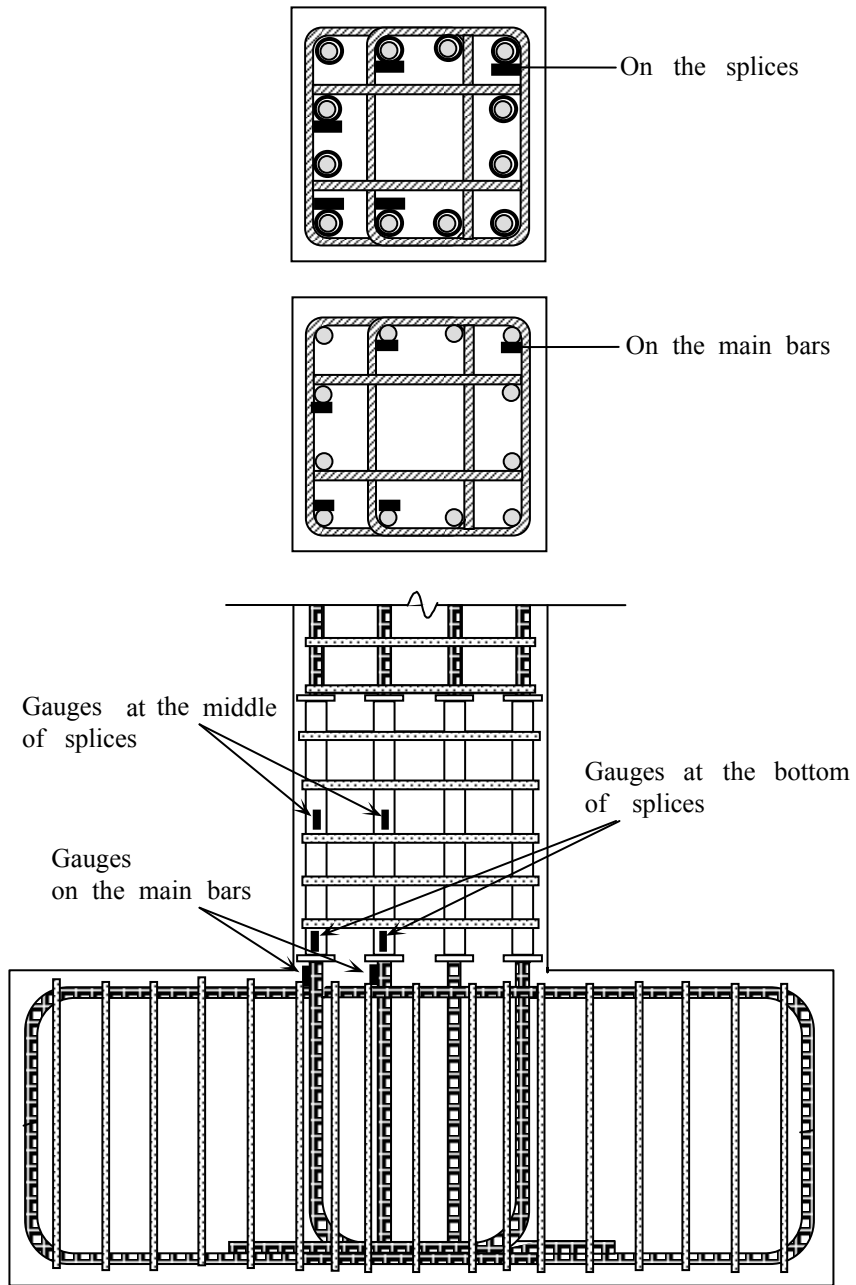


Figure 2.19: Strain Gauge Locations for Specimens PC1 and PC2

2.8 TEST PROCEDURE AND DATA ACQUISITION

The same test procedure was used for all specimens. Each test was conducted under displacement control rather than load control. A manual hand pump and a dial gauge were used to make it easier to control the test. During loading and unloading, continuous load-displacement curves were plotted to monitor the test.

At the peak of each displacement cycle, cracks on all faces of the column were marked using different colors according to the loading direction. Photographs were also taken at the same time. In order to make the cracks more visible, all column faces from the interface to a height of 4 ft. were white-washed, and 3 in. grid lines were drawn to record the progress and location of cracks (see Figure 2.20).

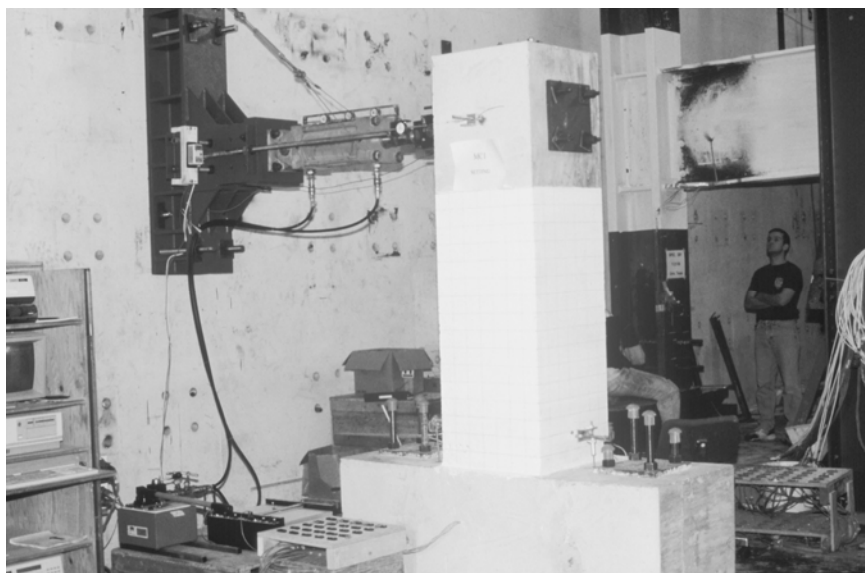


Figure 2.20: View of Specimen prior to Testing

Electronic data acquisition was performed using a high-speed scanner controlled by a microcomputer. A raw voltage reading from every measuring device was collected at each drift increment and stored on the microcomputer. The software called HPDAS2 was used to convert the raw voltages to engineering units.

CHAPTER 3

PRESENTATION OF TEST RESULTS

3.1 INTRODUCTION

Behavior of the specimens is described using plots of column shear (or applied lateral load) vs. drift, and cracking patterns. Column rotations at the base and curvatures are also discussed in this chapter. In addition, results of a single splice sleeve test that was performed after completion of all column tests are presented at the end of the chapter.

Test results indicated that Specimens PC2 and MC1 performed in a ductile manner. On the other hand, Specimen PC1 exhibited poor performance. Specimen PC1 showed slip of the spliced bars early in the test, which resulted in development of cracking near the top end of the splice sleeves. For Specimen PC2, a plastic hinge formed at the interface between the column and base element. When Specimen PC2 was loaded into the inelastic range, slip of the spliced bars was detected by popping noises from the splice region. However, significant strength was sustained until the end of the test.

3.2 COLUMN SHEAR FORCE - DRIFT ANGLE RELATIONSHIPS

Overall behavior of the specimens is demonstrated graphically through story shear-drift angle relationships. Figures 3.1 through 3.3 show the story shear-drift angle relationships for Specimens MC1, PC1 and PC2, respectively.

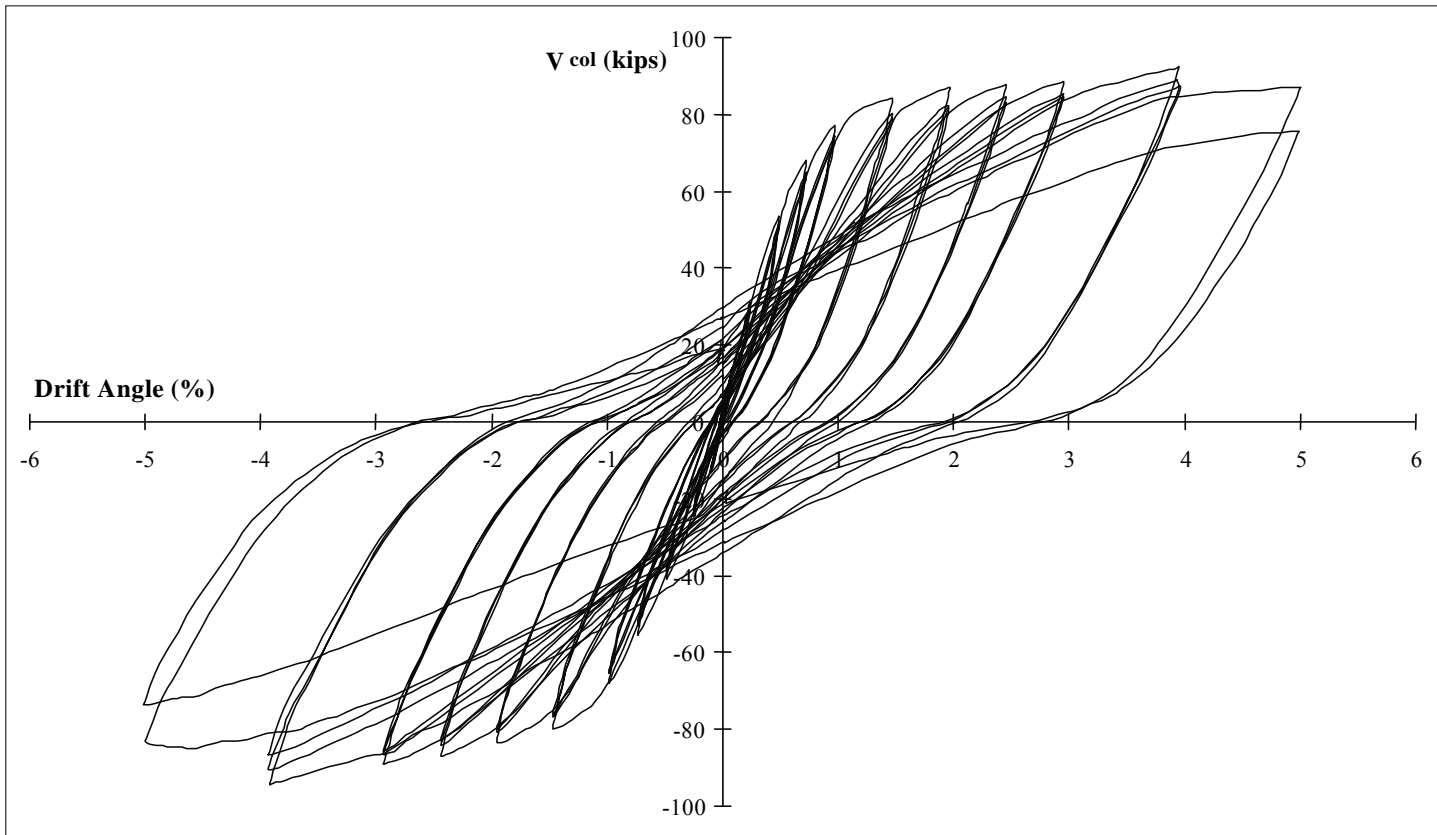


Figure 3.1: Shear Force versus Drift Angle for Specimen MC1

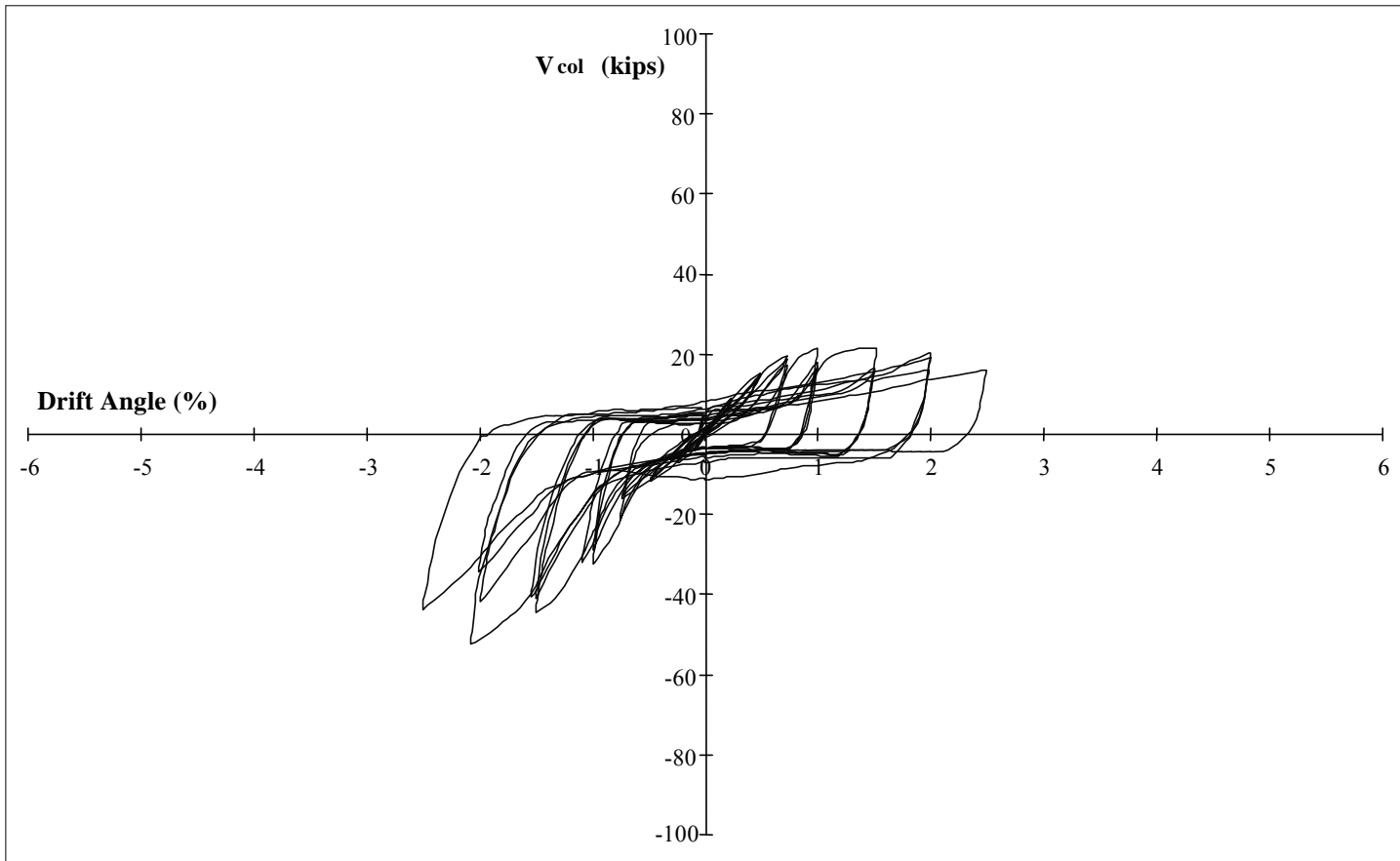


Figure 3.2: Shear Force versus Drift Angle for Specimen PC1

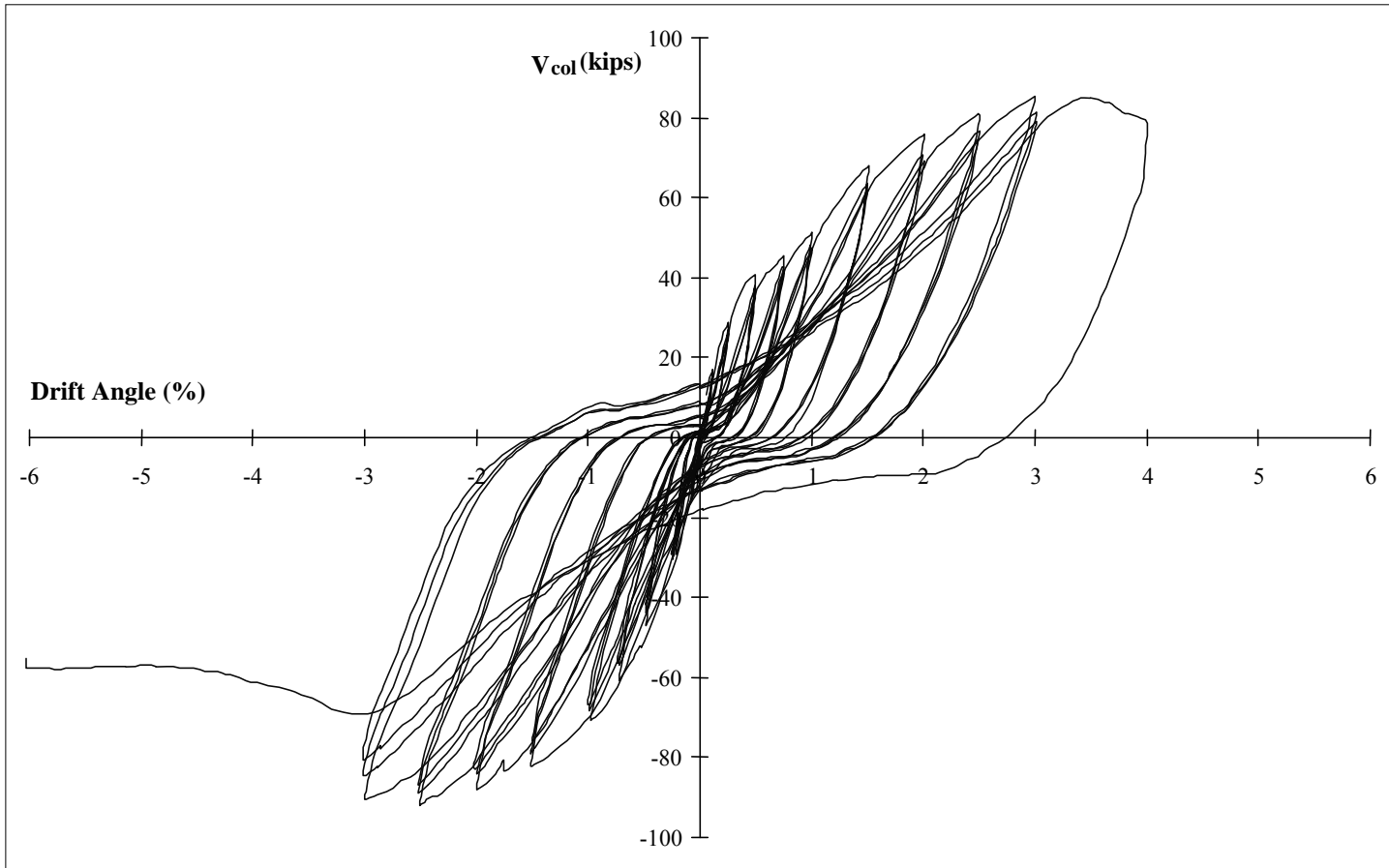


Figure 3.3: Shear Force versus Drift Angle for Specimen PC

Responses of specimens were plotted at the same scale in order to make comparisons. Positive and negative drift angles correspond with displacement of the column-tip away from and toward the reaction wall, respectively.

For all the specimens there was noticeable stiffness degradation between the first and second cycles at each displacement level. This stiffness degradation generally stabilized during the third cycle. Pinching of hysteresis loops occurred for all specimens, but was most pronounced for precast specimens.

The hysteresis loops obtained from Specimens MC1 and PC2 were very stable. Specimen MC1 reached an ultimate strength of 94.4 kips at 4 percent drift ratio, and Specimen PC2 attained an ultimate strength of 92.2 kips at 2.5 percent drift ratio. After reaching ultimate strength, both specimens maintained strength exhibiting only small reductions through large displacements.

For Specimen PC1, cracks formed near the top of the splice sleeves, approximately 20 in. above the column-base interface. The hinge resulted primarily from slip of the column bars in the splice sleeves. Movement of the spliced bars was noticed even during very early drift ratios resulting in small peak loads for each cycle (see Fig. 3.2). Failure of Specimen PC1 was indicated by a discernible low strength during the first cycle to 2.5 percent drift ratio. This deterioration in stiffness and strength was accompanied by bond failure of the spliced bars in the splice sleeves.

For Specimen PC2, although there was gradual degradation of stiffness during the test, the shape of the hysteresis loops remained relatively stable up to drift ratios of at least 3 percent. The pinching of loops was mainly associated with

slip of the spliced bars, which resulted in an increase in the interface crack width between the column and base element. Stiffness deterioration in the column element became significant only when drift ratios were in excess of 3.0 percent. During the first half cycle to 4.0 percent drift ratio, a reduction in strength was noticed. While loading to 4.0 percent drift ratio in the negative direction, a substantial reduction in strength and stiffness was exhibited. Therefore, the scheduled loading cycle was terminated after the first cycle of 4.0 percent drift ratio. Thereafter the specimen was monotonically loaded to the displacement limit of the loading system, which corresponded with approximately 6 percent drift ratio. As shown in Figure 3.3, load stabilized at approximately 57 kips, which was 63 percent of the maximum load capacity.

3.3 OBSERVED CRACKING AND DAMAGE

Crack patterns are sometimes helpful in visually assessing damage during a given loading cycle. Figures 3.4 through 3.9 show crack patterns on the column elements at selected drift ratios and at the end of each test.

In general, the most severe concrete cracking and spalling occurred in or around the lower end of the columns, where plastic hinges were anticipated to form adjacent to the base element. Cracks were marked at the end of the first and last cycles of each drift ratio. Most cracks, however, developed during the first cycle of each drift ratio, and only a few during the following two cycles. The surfaces of the column elements were painted with whitewash, and grid lines with 3-in. spacing were also drawn horizontally and vertically on all column faces to facilitate crack marking.

Initial cracking in all specimens was developed at the interface between the column and base element. Significantly different crack patterns were observed for column faces perpendicular versus parallel to the loading direction. On faces perpendicular to the loading direction, horizontal flexural cracks dominated and spalling occurred across the column width. On faces parallel to the loading direction, diagonal cracks were predominant.

Construction joints in the precast specimens were sound throughout both tests (i.e. no perceptible sliding occurred at these joints). Modes of failure and major crack development are discussed for each specimen in the following subsections.

3.3.1 Specimen MC1

The first crack was noticed at the interface between the column and base element during the first cycle to 0.1 percent drift ratio. Maximum shear during that cycle was 14.3 kips. During the first set of cycles, these interface cracks initiated from both sides of the column and propagated to join together. During the 0.25 percent drift cycles, flexural cracks developed up to 30 in. above the column-base interface. These cracks were well distributed over the anticipated plastic hinge region from the interface to 20 in. above the base element. At the end of 0.25 percent drift cycles, cracks located 9 in. above the interface started to incline. The maximum crack-width opening at the interface was approximately 0.01 in. During the 0.5 percent drift cycles, vertical cracks developed between

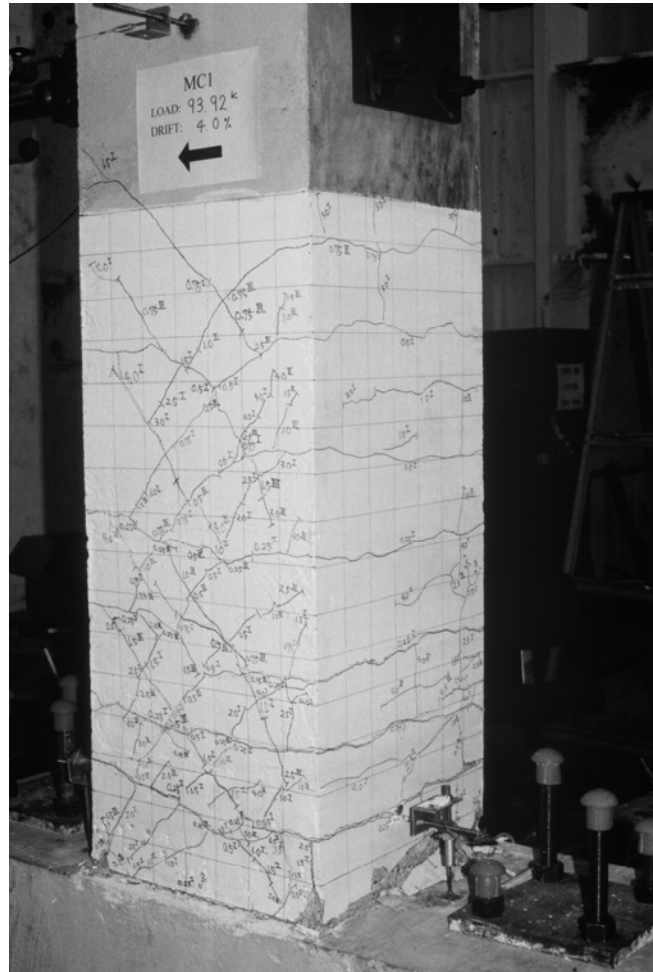


Figure 3.4: Crack Patterns for Specimen MC1

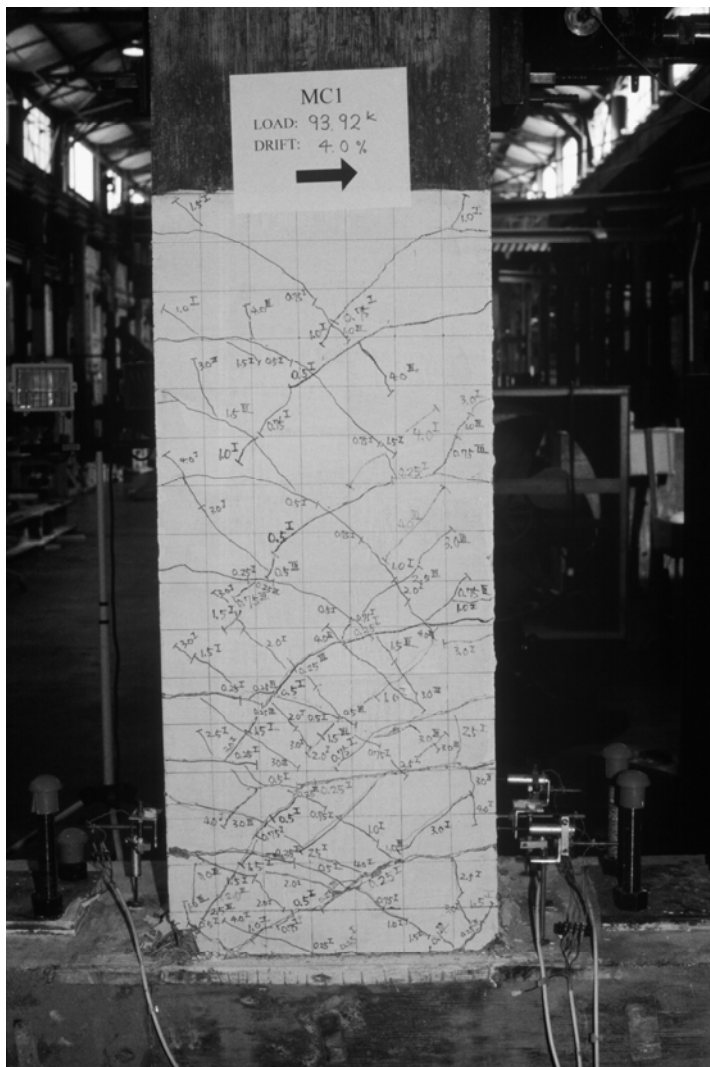


Figure 3.5: Specimen MC1 at Failure

horizontal cracks located on faces perpendicular to the loading direction. On faces parallel to the loading direction, new inclined cracks developed up to a 40-in. height. At 1.0 percent drift ratio, concrete at the column corners began to spall. The crack width of the interface was approximately 0.05 in. at this stage. At 1.5 percent drift ratio, strain gauges attached to the column longitudinal reinforcing bars indicated yielding, and stiffness degradation was evident. The maximum shear at this drift ratio was approximately 77 kips. Through the 2 percent drift ratio cycles, no major new cracks developed, but the width of cracks located at the interface and at 8.5 in. above the interface increased substantially. Figure 3.4 shows the crack patterns for Specimen MC1 at the end of the cycles to 2 percent drift ratio. For the entire test, the maximum lateral load recorded was 94.4 kips at a 4 percent drift ratio in the negative loading direction. The peak load for the first cycle of 5 percent drift ratio reached approximately 90 percent of the maximum load recorded for the previous drift ratio. Testing was discontinued following the second cycle to 5 percent drift ratio.

During testing there was no significant stiffness degradation noted until the end of the test. No visible cracks were found in the base element. Most concrete crushing and spalling, which occurred in the final stages of loading (5.0 percent drift ratio cycles), was concentrated along the flexural faces of the column near the base. Some column bars were even exposed at the end of the test. Figure 3.5 shows the crack patterns and damage sustained by the end of the test.

3.3.2 Specimen PC1

Initial cracking was simultaneously developed at the column-base interface and near the top end of the splice sleeves during 0.1 percent drift ratio cycles. At 0.25 percent drift ratio, the width of the crack approximately 20 in. above the interface was approximately 0.03 in. Because this location was near the top end of the splice sleeves, it indicated that column longitudinal bars slipped in the splice sleeves. The opening of this crack almost doubled at 0.5 percent drift ratio, and almost 60 percent of the crack width remained after removal of load. Because a substantial portion of the column deformations was concentrated in this crack, no other significant crack except the interface crack developed.

During the 1.0 percent drift-ratio cycles, the maximum load experienced was 32.3 kips, which was less than half the peak load developed by Specimen MC1 at the same drift ratio. Due to the substantial slip of the spliced bars, degradation of column stiffness was evident after the first cycle to 1.5 percent drift ratio. At 2.0 percent drift ratio, the maximum load obtained was 52.5 kips, which was 60 % of the peak load of 87 kips at the same drift ratio for Specimen MC1. Testing was terminated after the first cycle to 2.5 percent drift ratio because of the strength loss in the specimen.

At the end of the test, the specimen showed clear indications of splice failure. No yielding of longitudinal reinforcement was detected. Figure 3.6 shows the specimen after completion of the test. In addition, Figure 3.7 shows the crack opening at the top of the splice sleeves.

After completion of the test, the portion of the column element above the splice sleeves was removed by cutting the longitudinal reinforcing bars. Two of the splice sleeves were separated from the remaining portion of the column by chipping away the surrounding concrete. Cutting open the grout sleeves indicated that the sleeves were not completely filled. There was a gap found between the top surface of the grout and the end plate of each sleeve that measured from $3/8$ to $1/2$ in. The location of the top grout outlet may have contributed to the failure to fill the sleeves.

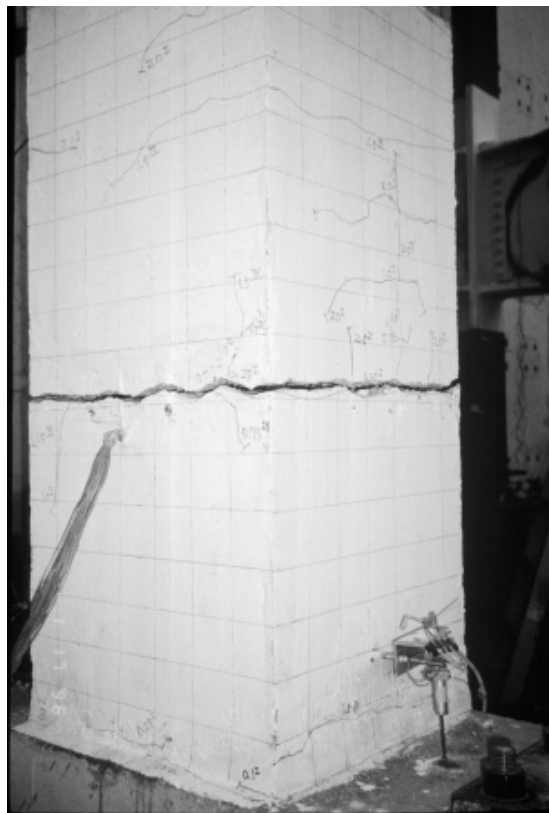


Figure 3.6: Failure of Specimen PC1

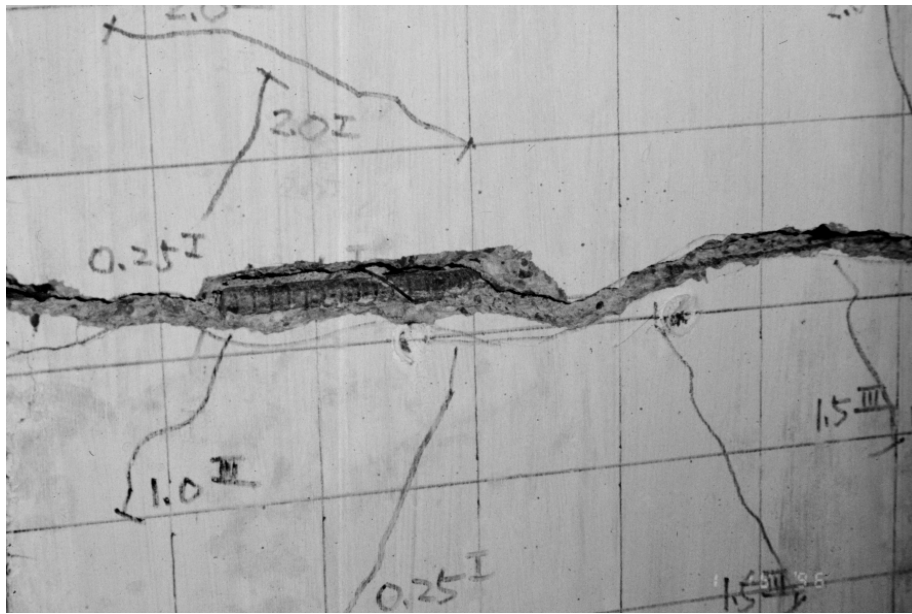


Figure 3.7: Crack Opening at the Top of Splice Sleeves (Specimen PC1)

Examination of the sleeves removed from the specimen also indicated segregation of the grout ingredients. Cement paste was more prevalent near the top of the splice sleeves, while sand was concentrated near the bottom of the sleeves. It was hypothesized that the space between the spliced bars and inside wall of the splice sleeve was too small to accommodate pumping of the grout without segregation.

3.3.3 Specimen PC2

Like the other specimens, the first crack developed at the interface between the column and base element. During 0.1 percent drift-ratio cycles, no other cracks developed. The crack at the top of the splice sleeves developed at 0.25 percent drift ratio, but the crack opening was approximately one fourth of the

crack width at a similar location in Specimen PC1. Up through 0.75 percent drift ratio, several flexural cracks developed up to approximately 40 in. above the interface. The width of the interface crack was approximately 0.02 in., but the crack width near the top of the splice sleeves remained less than 0.02 in. Also, at this drift ratio, strain readings indicated yielding of a corner longitudinal reinforcing bar at the interface. The maximum load at this drift ratio was 60.9 kips which was approximately 90 percent of the load at the same drift ratio for Specimen MC1.

Column secant stiffnesses for 0.5 to 1.0 percent drift ratios were larger for the negative direction than for the positive direction. Also, the interface crack width at zero load increased with increasing drift ratio. The increasing crack width at the interface was accompanied by pinching of the hysteresis loops after 0.5 percent drift ratio.

At 0.75 percent drift ratio, additional cracks formed in the column up to 39 in. above the base; some cracks were inclined. During loading to 1.5 percent drift ratio, slip of the spliced bars was heard almost continuously. At this stage of loading, the extreme longitudinal column bars in tension yielded. Concrete in compression at the corners of the column crushed at 2.5 percent drift ratio. The specimen was loaded to 4.0 percent drift ratio in the positive direction then to approximately 6 percent drift ratio (the displacement limit of the test setup). During loading in the positive direction toward 4.0 percent drift ratio, maximum load of 84.8 kips was recorded at approximately 3.3 percent drift ratio. Load decreased to 78 kips as the column was displaced further to 4 percent drift ratio.

The maximum load achieved during the test was 92.2 kips at 2.5 percent drift ratio in the negative loading direction. This was nearly the same strength as developed by Specimen MC1. However, the strength of Specimen MC1 was developed at 4.0 percent drift ratio. The load at 5.0 percent drift ratio, which was 57.2 kips (approximately 37 percent less than the maximum load), remained unchanged until the end of the test.

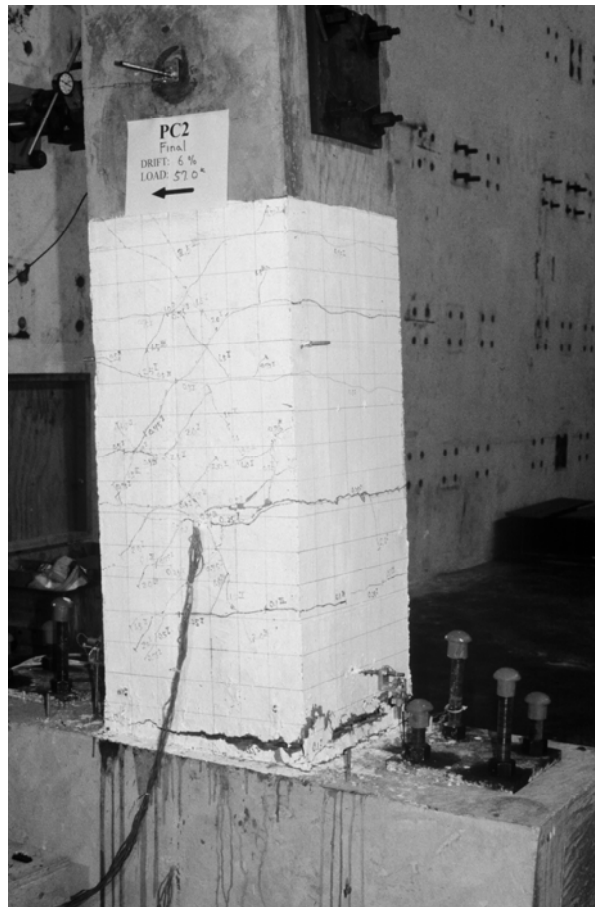


Figure 3.8: Crack Pattern and Damage in Specimen PC2



Figure 3.9: Photograph of Interface Crack (Specimen PC2)

Monotonic loading in the negative direction resulted in slip in the grout sleeves of the longitudinal bars extending out of the base element. The strain history for these bars indicated they reached yield and were at the onset of strain-hardening. Therefore, the splice sleeves were capable of resisting many cycles of load reversals, some of which reached yield of the longitudinal reinforcement. Following completion of the test, some of the spliced column longitudinal bars could be seen through the interface crack. Bars which had been pulled out of the bottom of the splice sleeves were surrounded by grout that was sheared through at the tops of the bar deformations. Figure 3.8 shows the crack patterns and damage sustained at 4.0 percent drift ratio. Figure 3.9 also shows the crack opening at the interface.

3.4 COLUMN ROTATIONS

For Specimens MC1 and PC2, the majority of column deformations occurred in the assumed plastic-hinge region that ranged from the interface to 20 in. above the base.

For Specimen PC1, most column deformations were concentrated at the crack near the top of the splice sleeves. Two linear potentiometers were used to collect data for rotation at the bottom of each column. They were located on opposite sides of the column element approximately 6 in. above the bottom of the column. Because the largest, most significant crack in the column of Specimen PC1 developed above the linear potentiometer locations, no useful data were available to calculate rotations at the base of the column. Therefore, rotations are reported only for Specimens MC1 and PC2. Two rotations were calculated for each column: the concentrated rotation at the column base, and the drift ratio expressed as an angle (referred to as the tip deflection angle).

Column-tip deflection angles were computed by dividing the column tip displacement (minus any horizontal sliding at the base) by the height of the column. Horizontal slip of the column element at the base corresponded with as much as 5 percent and 8 percent of the column-tip deflection for Specimen MC1 and Specimen PC2 respectively.

Table 3.1 lists the ratios of column base rotation to column-tip deflection angles for Specimens MC1 and PC2. The deformations required for calculation of the ratios were taken from the first cycle of each drift ratio. Reliability of

deformation data measured with linear potentiometers was questionable beyond 4.0 percent drift ratio.

Table 3.1: Ratios of Column Base Rotation to Column Tip Deflection Angle

| Drift Ratio (%) | Specimen MC1 | | Specimen PC2 | |
|--------------------|--------------|----------|--------------|----------|
| | Positive | Negative | Positive | Negative |
| 0.25 | 64.0 | 56.8 | 60.2 | 63.9 |
| 0.5 | 60.7 | 50.3 | 61.2 | 64.8 |
| 0.75 | 55.0 | 48.7 | 54.7 | 66.7 |
| 1.0 | 48.9 | 47.1 | 58.6 | 72.6 |
| 1.5 | 50.0 | 56.1 | 63.7 | 83.7 |
| 2.0 | 56.2 | 60.7 | 66.5 | 83.9 |
| 2.5 | 62.6 | 65.0 | 69.0 | 82.8 |
| 3.0 | 67.4 | 69.7 | 80.5 | 84.7 |
| 4.0 | 70.5 | 72.3 | 88.0 | 97.9 |

Data in Table 3.1 indicate that the contribution of deformations near the base of the column to the column-tip deflection initially decreased from approximately 60 percent to 48 percent for Specimen MC1 through 1.0 percent drift ratio, then increased to more than 70 percent at 4 percent drift ratio. The contribution of column deformations near the base to column-tip deflections for Specimen PC2 decreased slightly in the positive direction through 0.75 percent drift ratio then increased to 88 percent at 4.0 percent drift ratio. In the negative

direction the contribution increased throughout the test to 98 percent at 4.0 percent drift ratio.

Specimen MC1 initially exhibited a decreasing ratio of column base rotation to column-tip deflection angle because cracking spread to an increasing height with increasing drift ratio. The ratio increased for both specimens after yielding of longitudinal reinforcement occurred. The ratio increased more for Specimen PC2 because cracking was concentrated at the interface between the column and base elements instead of being distributed over a flexural hinge region, and because slip of bars in the splice sleeves was concentrated at the interface crack.

3.5 RESULTS OF AN INDIVIDUAL SPLICE SLEEVE TEST

Design of the precast specimens was based on the assumption that the grouted splice sleeves develop the necessary forces in the longitudinal reinforcing bars. In addition to tests on Specimens PC1 and PC2, a test of a single splice sleeve was performed to learn more about the behavior of the particular splice sleeve used in this study. The splice sleeve was fabricated with the same details used in Specimen PC2.

Figure 3.10 shows the test setup for the single splice sleeve test. It also illustrates the locations of transducers used to measure slip and elongation outside the splice sleeve of the spliced bars. Figure 3.11 shows the bar and surrounding grout that were pulled out from the splice sleeve during testing.

The splice specimen had one significant difference from the splice sleeves used in Specimen PC2. Because splice sleeves used in Specimen PC2 were

embedded in the column element before grouting was performed, the expansive grout could not easily escape around the reinforcing bars at the ends of the splice sleeve during expansion. Despite efforts to block the openings between the reinforcing bars and plates at the ends of the splice sleeve, grout oozed from the splice sleeve ends during curing.

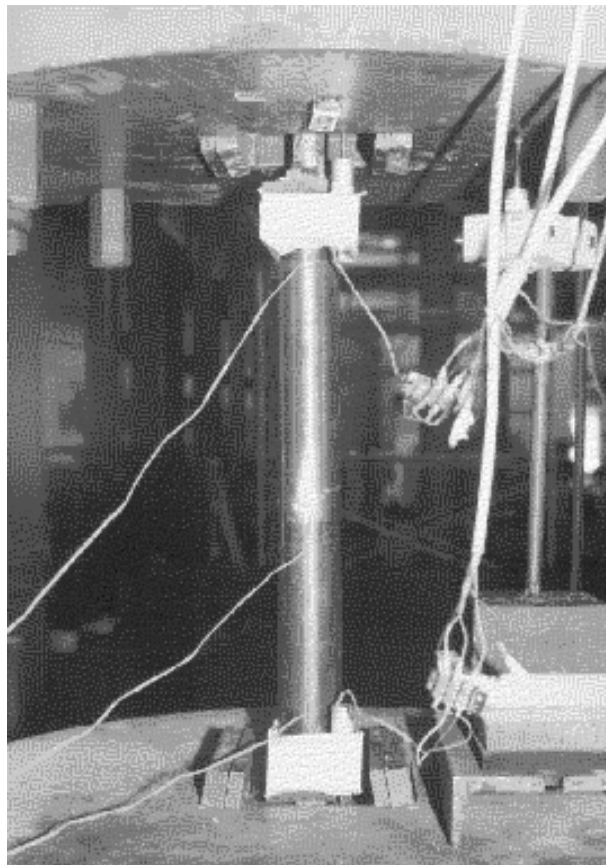


Figure 3.10: Test Setup for Single Splice Sleeve Test



Figure 3.11: View of Spliced Bar after Testing

Figure 3.12 shows the load-elongation plot from the splice sleeve test. Elongation was measured between points that were 5 in. apart. This was the distance between the upper end plate of the splice sleeve to the bottom of the top set of grips in the test machine. The dashed line in Figure 3.12 represents force in the reinforcing bars estimated for the maximum moment developed in Specimen PC2.

The plot also indicates that slip of the spliced bars initiated before yielding. The maximum load attained was approximately 14 percent higher than the load corresponding to nominal yield strength of the spliced bars, which was approximately 47 kips. The majority of elongation plotted in Fig. 3.12 was due to slip of the bars. Reduction in load after capacity was reached was quite gradual.

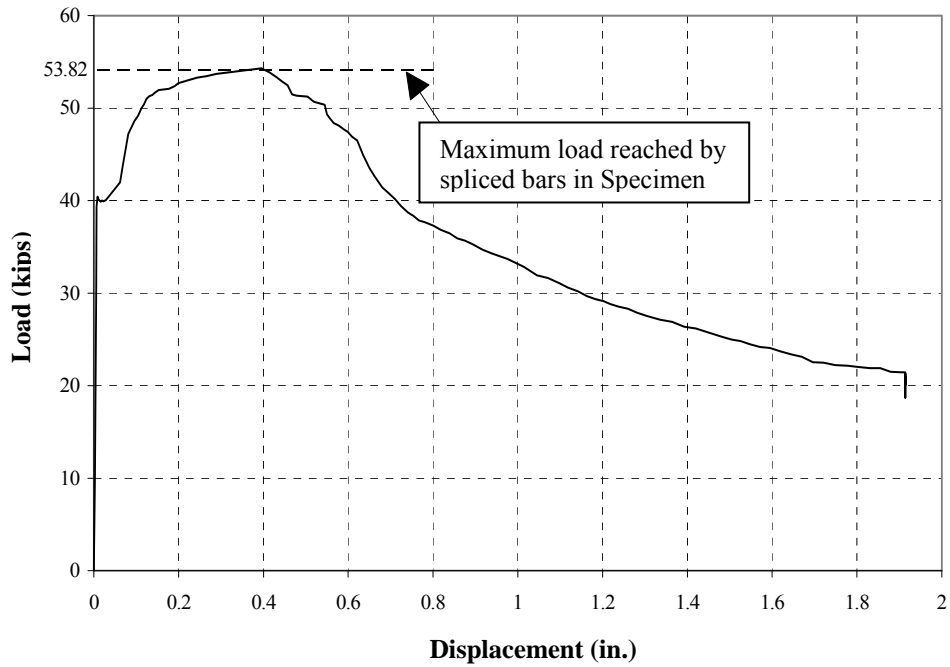


Figure 3.12: Load-Displacement Plot from Single Splice Sleeve Test

The plot shows that slip of the spliced bars starts before they reach their yield strength (approximately 50 kips). Strains obtained from the strain gauges attached on the splice sleeve were relatively small compared to overall elongation measured for the splice assembly. Most of the displacement was caused by slip of the spliced bars. The measured response after reaching maximum load indicates a very gradual reduction in strength.

CHAPTER 4

EVALUATION OF TEST RESULTS

4.1 INTRODUCTION

In the previous chapter, the overall behavior of the test specimens was presented. Comparisons of energy dissipation, residual drift, stiffness, and stiffness degradation are evaluated in this chapter. Data obtained from strain gauges attached to column longitudinal reinforcing bars are also presented and discussed.

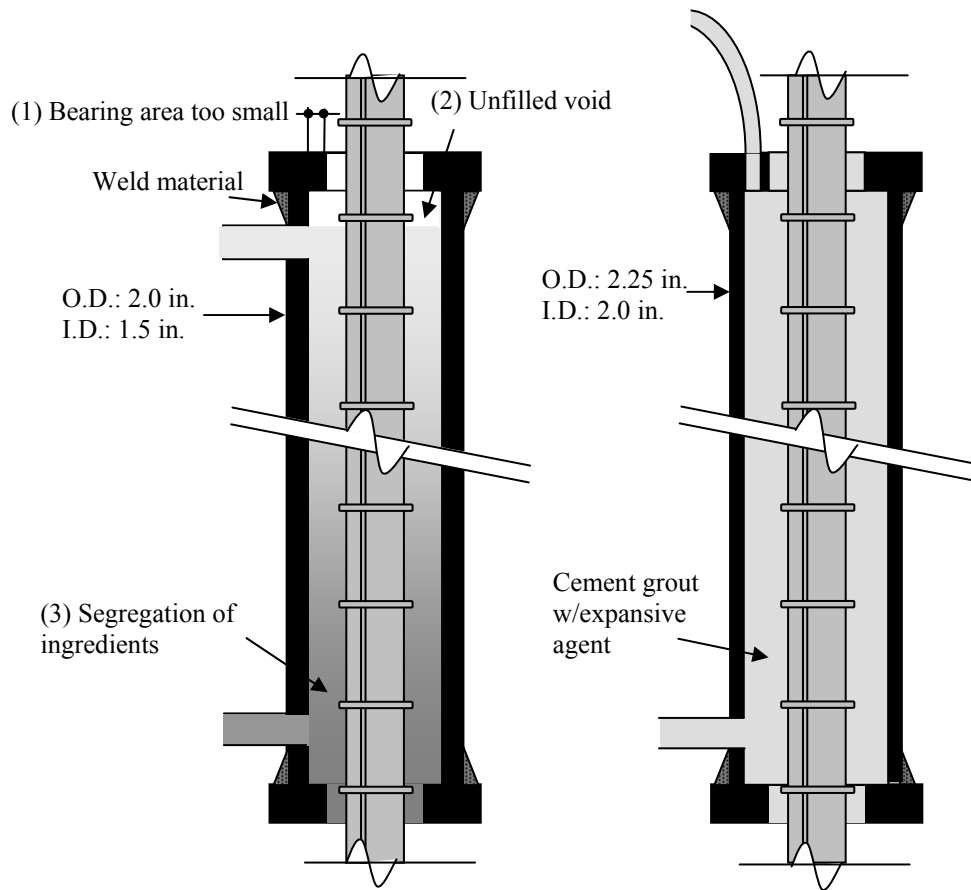
As discussed in Chapter 3, specimen PC1 performed very poorly compared to Specimen PC2. Only limited data from the test of Specimen PC1 were available for evaluation because cracking developed unexpectedly near the top of the splice sleeves instead of at the base of the column where most of the instrumentation was located. Therefore, due to a lack of comparable data, most evaluations will be made using data from Specimens MC1 and PC2. Problems encountered during fabrication and testing of Specimen PC1 will be discussed in Section 4.2.

4.2 PROBLEMS WITH PROTOTYPE SPLICE SLEEVE

The design of the splice sleeves used in Specimen PC1 was based on research by Einea et al. [4]. Their splice details were adopted for use in the splice sleeves incorporated in Specimen PC1. However, use of these details in Specimen

PC1 revealed some problems during grouting and testing that necessitated modification of the details and grouting procedures.

Figure 4.1 shows the problems encountered in the splice sleeve used for Specimen PC1. It also indicates the changes in the splice sleeve detail.



(a) Splice sleeve for Specimen PC1 (b) Splice sleeve for Specimen PC2

Figure 4.1: Comparison of the Splice Sleeves for Specimens PC1 and PC2

The first problem noted was the bearing area at the ends of each splice sleeve (Fig. 4.1(1)). The opening at each end of the splice sleeve was not sufficiently small to prevent the grout from extruding through the opening. In an actual structural member, the diameter of the splice hardware would be limited to avoid the addition of concrete cover. Instead of significantly increasing the diameter of the splice sleeve to increase the bearing area for the grout, a pipe with thinner wall thickness and higher steel strength was substituted for the original pipe splice used in Specimen PC1.

The second problem identified was the incomplete placement of grout (Fig. 4.1(2)). The location of the vent tube was primarily responsible for this problem. In order for the splices to perform as expected, the grout had to completely fill the void space. As mentioned in the previous chapter, the top edge of the vent tube in the splice wall was positioned $\frac{3}{8}$ in. beneath the end plate to avoid the fillet weld. The diameter of the vent tube was $\frac{1}{2}$ in. Consequently, the bottom edge of the tube was located $\frac{7}{8}$ in. away from the end plate. The grout was too fluid (slump was too high) to fill this space above the vent tube inside the splice sleeve. During testing of Specimen PC1, this void at the top of the splice sleeve accounted for slip of the column bars at the top of the splice sleeve.

The third problem identified was associated with the grout material itself (Fig. 4.1(3)). The grouting material used for Specimen PC1 was a Euclid commercial non-shrink grout that included sand. During the grouting procedure, the tight space inside the splice sleeve impeded the flow of the sanded grout,

resulting in settlement of the sand at the bottom of the splice sleeve. The sand sediment then acted like a strainer. During inspection of the splice sleeve after testing, the top portion of the grout appeared to be composed mainly of relatively weak cement paste. Most of the sand was found near the bottom of the splice sleeve.

The problems mentioned resulted in a major crack near the top of the splice sleeves in Specimen PC1. As a result, modifications in the splice sleeve details were made as shown in Figure 4.1(b).

First, the space between the inside wall of the pipe and the spliced bar was increased. To accomplish this, the outside diameter of the pipe was increased as much as the concrete cover would allow, and the thickness of the pipe wall was reduced to 1/8 in. by using a higher-strength material. These changes resulted in a 0.5 in. increase in the inside diameter of the pipe.

Second, the location of the vent tube was moved from the sidewall of the pipe to the top end plate. In order to ensure complete filling of the pipe with grout, a smaller hole was drilled in the top end plate, and a clear plastic tube was attached to the hole. This plastic tube had a small diameter but was large enough to serve as an outlet for air and grout.

The last change involved replacing the original grout material with a cement grout containing no sand. Removing the sand from the grout made the grouting procedure much easier by increasing the slump of the grout. In addition, an expansive agent was included in the grout. The primary reason for using the expansive agent was to help fill the void completely. A secondary effect of adding

the agent was the increase in initial confining pressure provided around the spliced bars. However, the use of the expansive agent required extra caution in measuring the mix proportions to avoid reduction in grout strength.

4.3 RESPONSE ENVELOPE CURVES

During testing, psuedo static reversed cyclic loads were applied to simulate dynamic cyclic loading during an earthquake. It is often useful to examine the monotonic response of a connection for insight into the strength, stiffness, and ductility. Response envelopes for Specimens MC1 and PC2 were constructed by connecting the points corresponding to peak response for the first cycle of each drift ratio to examine monotonic response.

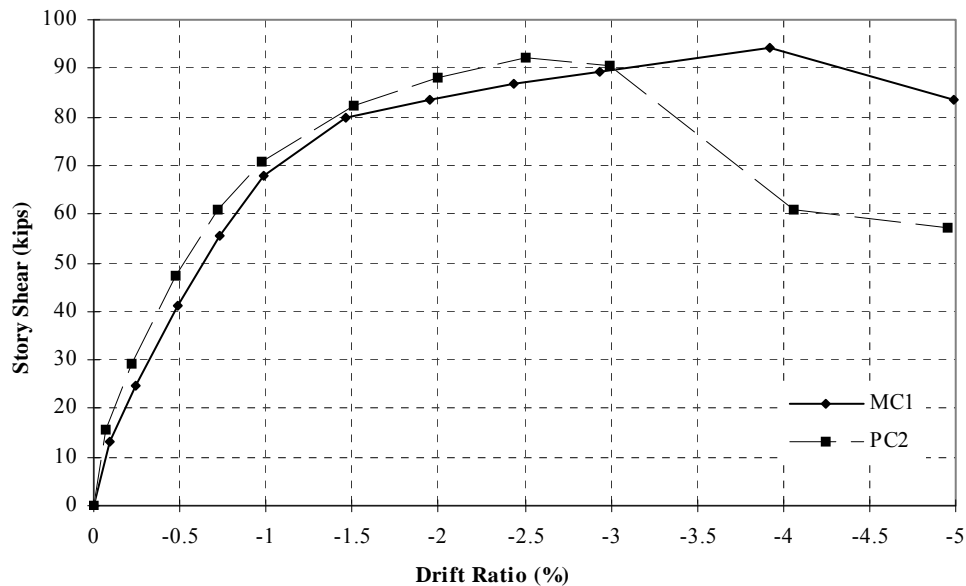


Figure 4.2: Response Envelopes

Figure 4.2 shows the response envelope curves for Specimens MC1 and PC2 for loading in the negative direction. Envelopes for the positive loading direction are very similar to those for the negative loading direction up to the 4.0 percent drift ratio. However, the positive loading cycles for Specimen PC2 did not continue beyond the 4.0 percent drift ratio. As a result, the negative loading direction was chosen for comparison.

The response envelopes for both specimens are very similar up to approximately 2.5 percent drift ratio. Initial stiffness of Specimen PC2 was slightly higher than that of Specimen MC1. Specimen PC2 reached ultimate strength at 2.5 percent drift ratio. The strength of Specimen PC2 decreased rapidly beyond 3.0 percent drift ratio due to splice deterioration.

For Specimen MC1, ultimate strength was obtained at a drift ratio of approximately 3.9 percent. After reaching ultimate load, Specimen MC1 experienced relatively slow reduction in strength compared to Specimen PC2.

Table 4.1 lists the calculated and measured lateral load capacities. Calculated capacities are based on measured material properties with no consideration of strain hardening in the steel. The steel strength was obtained from monotonic tensile coupon tests, and concrete compressive strength was based on cylinder tests performed on the first day of testing. The measured lateral load capacities are also listed in Table 4.1. The table indicates that both specimens reached their calculated lateral load capacities. Specimen MC1 had a slightly higher capacity than Specimen PC2.

Table 4.1: Calculated and Experimental Strength of Specimens MC1 and PC2

| Specimen | Calc. Lateral load Capacity $P_{u,calc}$ (kips) | Measured Lateral load Capacity $P_{u,exp}$ (kips) | $\frac{P_{u,exp}}{P_{u,calc}}$ | Drift Ratio@ $P_{u,exp}$ | Max. Drift Ratio (%) |
|----------|--|--|--------------------------------|--------------------------------|-------------------------------|
| MC1 | 87.1 | 94.4 | 1.08 | 4.0 | 5.0 |
| PC2 | 87.7 | 92.2 | 1.05 | 2.5 | 4.0 |

Stiffness of Specimen PC2 was larger than that of Specimen MC1 up to ultimate load. However, Specimen PC2 exhibited less ductility, indicating less capacity for energy absorption. Further comparisons of stiffness will be discussed in Section 4.5.

4.4 HYSTERETIC BEHAVIOR

4.4.1 Energy Dissipation

Large amounts of energy are released during an earthquake. Some of this energy is transformed into potential energy that is absorbed by the structure as strain energy. Deformations of the structure are responsible for most of the energy absorption/dissipation mechanism. It is important to study the performance of the specimens under large cyclic deformations to assess their energy dissipation

characteristics. The total amount of energy dissipated for each specimen is obtained by calculating the area inside the hysteresis loops described by the story shear-interstory drift curves.

Figure 4.3 shows cumulative energy dissipated by Specimens MC1 and PC2 for the positive loading direction. As implied by the load-displacement relationships, Specimen MC1, which demonstrated more ductile behavior, dissipated more energy than Specimen PC2. Beyond 1.0 percent drift ratio, Specimen PC2 showed a slower increase in cumulative energy dissipation than Specimen MC1. This difference can be attributed primarily to the pinching observed in the load-displacement response of Specimen PC2. Pinching was primarily due to slip of the longitudinal bars through the splice sleeves. However, beyond 2.5 percent drift ratio, increases in cumulative energy dissipation were approximately the same for both specimens.

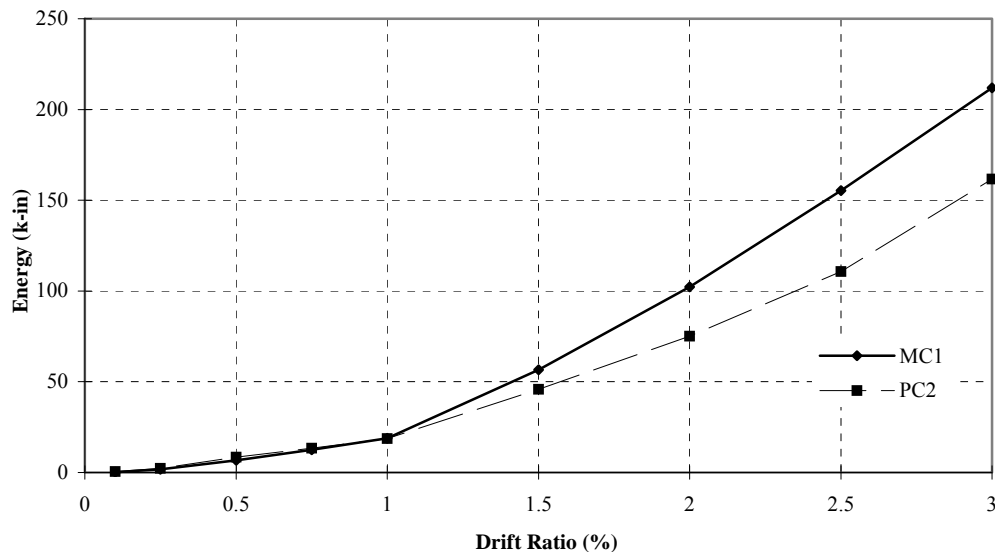


Figure 4.3: Cumulative Energy Dissipated

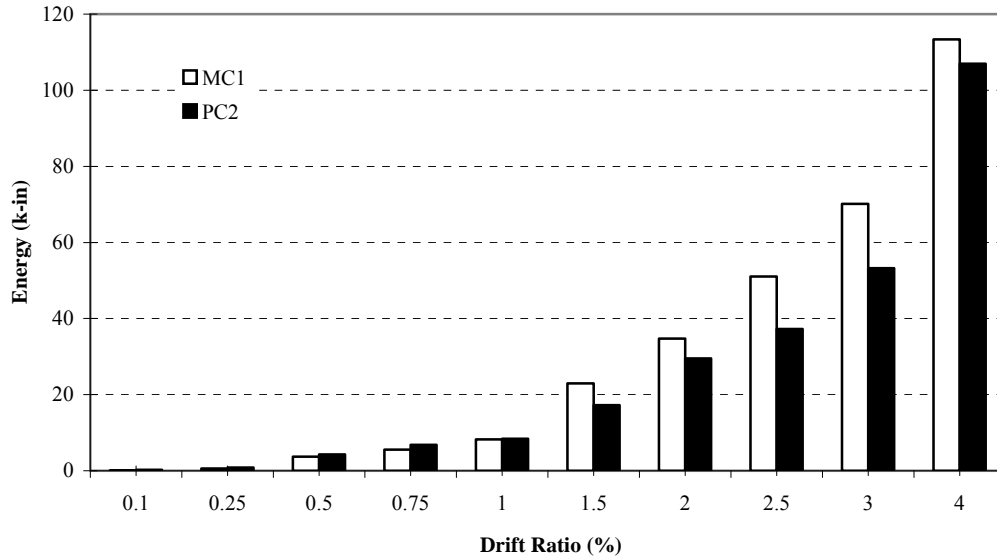


Figure 4.4: Energy Dissipated in the First Cycle of Each Drift Ratio

Figure 4.4 illustrates the energy dissipated during the first cycle of each drift ratio. The energy dissipated up to 1.0 percent drift ratio was minimal for both specimens. At approximately 1.0 percent drift ratio for Specimen MC1, nonlinear response was initiated by yielding of the longitudinal reinforcing bars. As drift ratio increased beyond 1.0 percent, the energy dissipated in each cycle increased approximately exponentially for both specimens. Based on Figure 4.3, the energy dissipated in the first cycle at each drift ratio accounts for approximately 30 to 50 percent of the total energy dissipated.

Specimen PC2 demonstrated a large increase in dissipated energy during the first cycle to 4.0 percent drift ratio. The increase was related to the sudden unloading of the specimen accompanied by little reduction in displacement. The tensile reinforcement associated with positive loading was not loaded further, the

spliced tensile reinforcement associated with negative loading maintained significant resistance (approximately 60% of maximum load) beyond 6.0 percent drift ratio.

4.4.2 Equivalent Viscous Damping Ratio

Hysteretic damping is an important parameter influencing the ability of a structure to dissipate energy during dynamic excitation. The equivalent viscous damping ratio H_{eq} can be obtained by computing the ratio of dissipated energy to strain energy of an equivalent linear system divided by 2π . This definition is illustrated in Figure 4.5. The equivalent viscous damping ratio normalizes hysteretic damping with respect to viscous damping, and reflects the amount of pinching in the hysteresis loops.

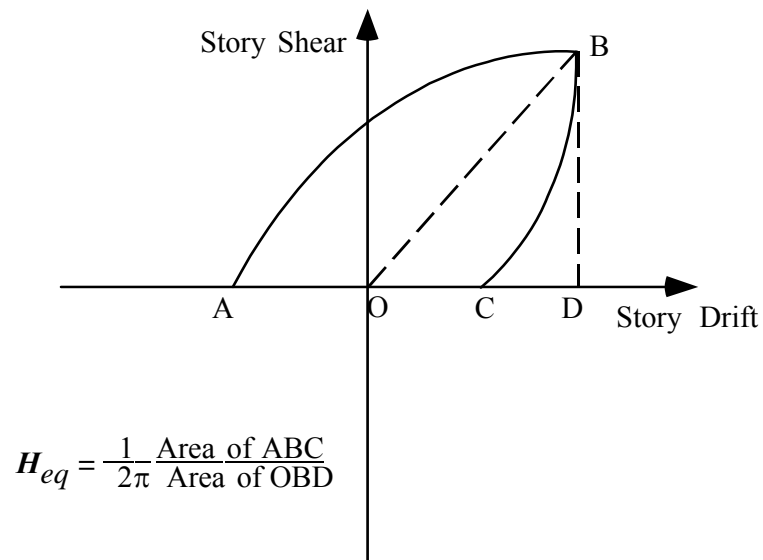


Figure 4.5: Definition of Equivalent Viscous Damping Ratio, H_{eq}

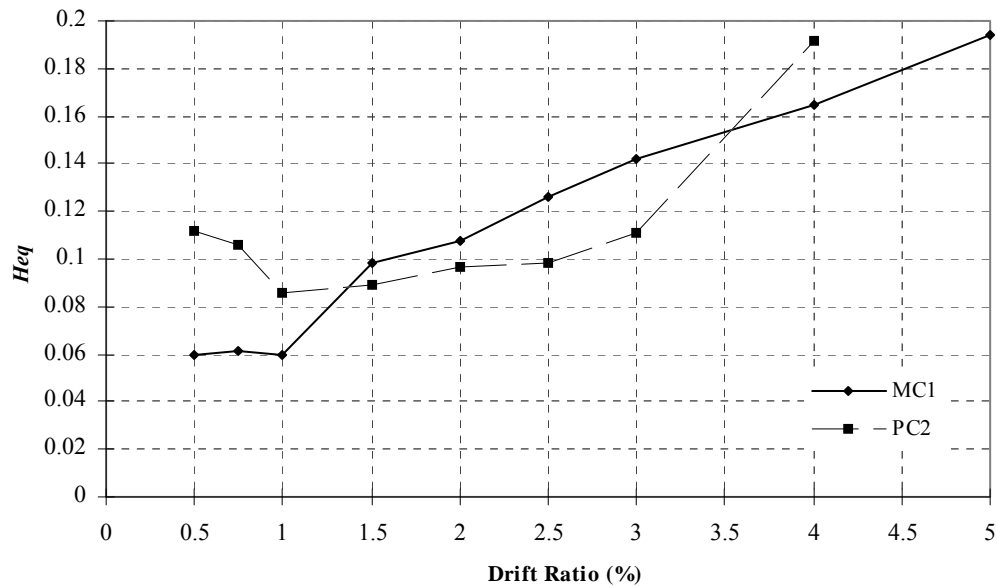


Figure 4.6: Equivalent Viscous Damping Ratio

Figure 4.6 shows the equivalent viscous damping ratios for Specimens MC1 and PC2 for 0.5 percent drift ratio and higher. The values for lower drift ratios were not included here because response through 0.25 percent drift ratio was nearly linear.

Up to 1.0 percent drift ratio, the equivalent viscous damping ratios for Specimen PC2 were higher than those for Specimen MC1 because the elastic stiffness of Specimen PC2 was higher during low drift ratios. However, after 1.0 percent drift ratio and up to 3.0 percent drift ratio, the values of H_{eq} for Specimen PC2 were smaller than those for Specimen MC1 primarily due to the pinching observed in the response of PC2. As the drift ratio was increased from 3.0 percent to 4.0 percent, H_{eq} for Specimen PC2 increased more. This increase is related to

the steeper unloading curve for Specimen PC2, which is likely related to slip of reinforcement in the splice hardware during unloading.

4.5 COMPARISON OF STIFFNESS AND DUCTILITY

4.5.1 Secant Stiffness and Ductility

Secant stiffnesses are compared in this section for Specimens MC1 and PC2. Estimates of ductility are also presented.

Using the response envelope curve, the secant stiffness assumed to represent the cracked, elastic stiffness of a specimen is estimated as shown in Figure 4.7. Using code-based lateral load capacity, a strength reduction factor of 1.0, and actual material and geometric properties of the specimen, ultimate lateral load strength P_u is calculated. These values are shown in the second column of Table 4.2 for Specimens MC1 and PC2. The displacement corresponding to $0.75P_u$, which is called Δ^* , is obtained from the response envelope curve. The slope of the line passing through the origin and the point defined by $0.75P_u$ and Δ^* is taken as the secant stiffness.

$$K_{\text{sec}} = \frac{0.75P_u}{\Delta^*} = \frac{P_u}{\Delta_y}$$

The intersection of the extension of that line and a horizontal line corresponding to the calculated lateral load capacity P_u is taken as the yield displacement Δ_y . The yield displacements for Specimens MC1 and PC2 are listed in the fourth column of Table 4.2.

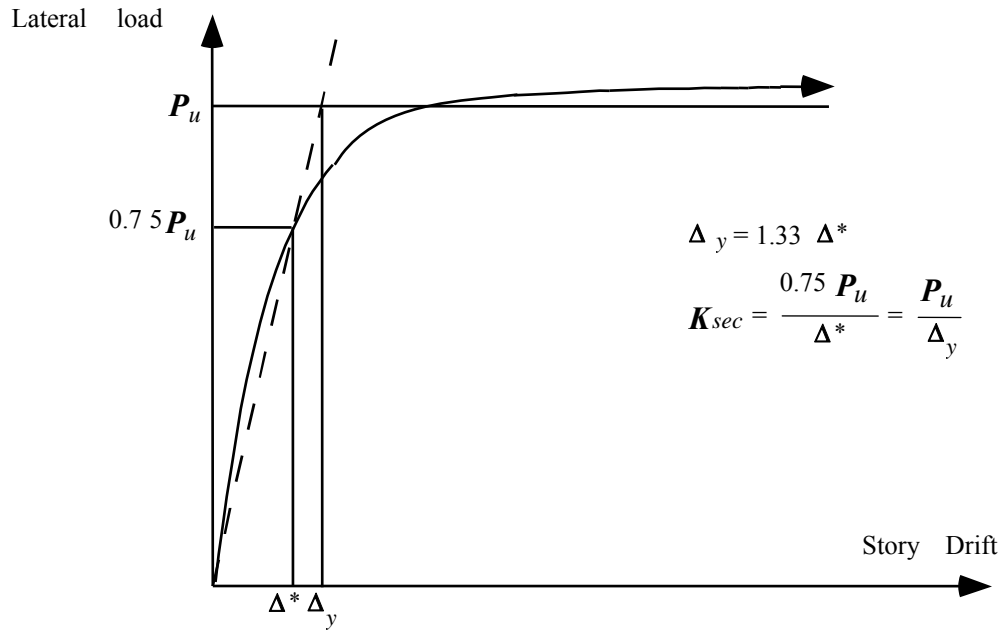


Figure 4.7: Definition of Secant Stiffness and Yield Displacement

An estimate of displacement ductility is computed as

$$\mu = \frac{\Delta_u}{\Delta_y}$$

where Δ_u is the maximum measured drift. Ductility ratios are listed in the fifth column of Table 4.2.

Table 4.2: Stiffness and Ductility of Column Specimens

| Specimen | Calculated Lateral load $P_{u,calc}$ (kips) | Secant Stiffness K_{sec} (k/in) | Yield Displacement Δ_y (in) | Ductility μ |
|----------|---|---|--|--------------------|
| MC1 | 87.1 | 163.7 | 0.53 | 5.6 |
| PC2 | 87.7 | 134.5 | 0.65 | 3.7 |

As shown in Table 4.2, the secant stiffness of Specimen MC1 was greater than that of Specimen PC2. The lower stiffness of Specimen PC2 is attributed to splice slip that was detected at approximately 0.75% drift ratio.

The maximum plausible earthquake-imposed story drift ratio for a column would be on the order of 3 percent [7]. Displacements beyond this limit are likely to lead to serious overall frame instability. According to Table 4.2, the yield displacement of Specimen PC2, which corresponded with approximately 1.0 percent drift ratio, was larger than that of Specimen MC1. This is because yielding of the spliced bars was accompanied by slip of the reinforcement in the splice devices. For an actual frame structure, the story drift ratio causing yielding of column longitudinal reinforcement would be higher. In this study, only column and splice deformations contributed to the overall drift. For a frame system, beam and joint deformations would also contribute to story drifts.

Due to the different mechanisms leading to strength deterioration of the column specimens, Specimen PC2 exhibited a relatively small displacement ductility ratio. Bond failure of the spliced bars in Specimen PC2 was prominent after ultimate strength was reached at 2.5 percent drift ratio. Bond failure resulted in rapid stiffness and strength deterioration.

4.5.2 Stiffness Degradation

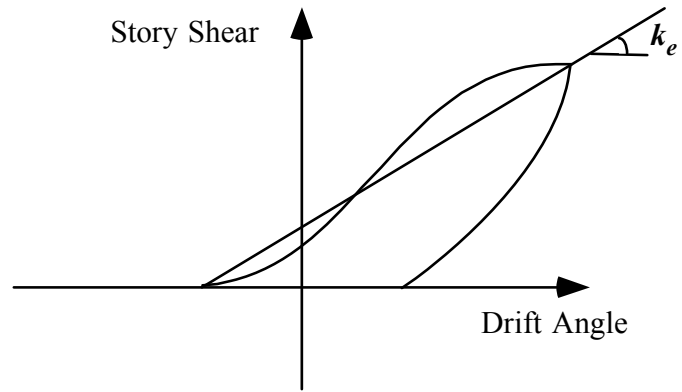
All reinforced concrete members experience some stiffness degradation during reversed cyclic loading. Stiffness degradation reduces hysteretic damping because the area under the load-displacement curve decreases. Stiffness

degradation is attributable to opening and closing of cracks, sliding at crack interfaces, concrete crushing and spalling, and bond degradation.

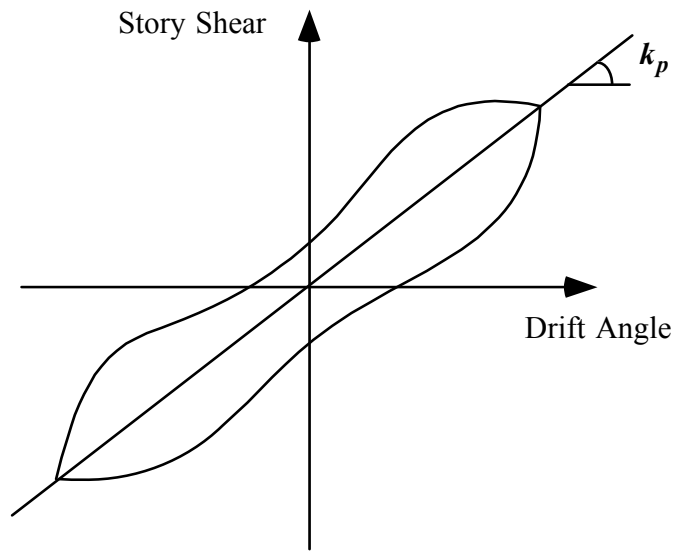
Stiffness of subassemblages can be defined through story shear-drift angle relations. Definitions of equivalent stiffness and peak-to-peak stiffness are shown in Figure 4.8. Equivalent stiffness K_e can be computed for each half cycle in each loading direction. As shown in Figure 4.8(a), K_e is the slope of the line connecting the response points corresponding with zero story shear and maximum drift angle for the given loading cycle.

Because the tests were performed under displacement control, the point corresponding with zero story shear usually occurs in the previous half cycle. Therefore, a hysteresis loop for elasto-plastic behavior and another with severe pinching will have the same equivalent stiffness as long as the zero story shear and peak displacement values are the same.

Peak-to-peak stiffness K_p can be computed for each loading cycle. Figure 4.8 (b) shows a line connecting points corresponding with maximum positive and negative drift angles. The slope of this line is the peak-to-peak stiffness. Due to the definitions for stiffness shown in Fig. 4.8 and the nature of the hysteresis loops, peak-to-peak stiffness values are typically larger than equivalent stiffness values. Equivalent stiffness facilitates comparisons between response half-cycles for a given loading direction, while peak-to-peak stiffness values provide for comparisons between full response cycles.



(a) Equivalent Stiffness



(b) Peak-to-Peak Stiffness

Figure 4.8: Definition of Stiffnesses

4.5.2.1 Equivalent Stiffness

Stiffness deterioration for Specimens MC1 and PC2 following each half cycle of response are shown through equivalent stiffness vs. drift ratio plots in Figure 4.9. The stiffness values presented are based on the first load cycle at each drift ratio. Both specimens consistently exhibited greater equivalent stiffness for the first positive half cycle compared with the first negative half cycle. For a given drift level, resistance in the negative loading direction was affected by damage induced during loading to a new maximum drift level in the positive loading direction. The first cycle to a new maximum drift level also induced a larger residual drift in the positive loading direction. Both of these affected the equivalent stiffness for the negative loading direction.

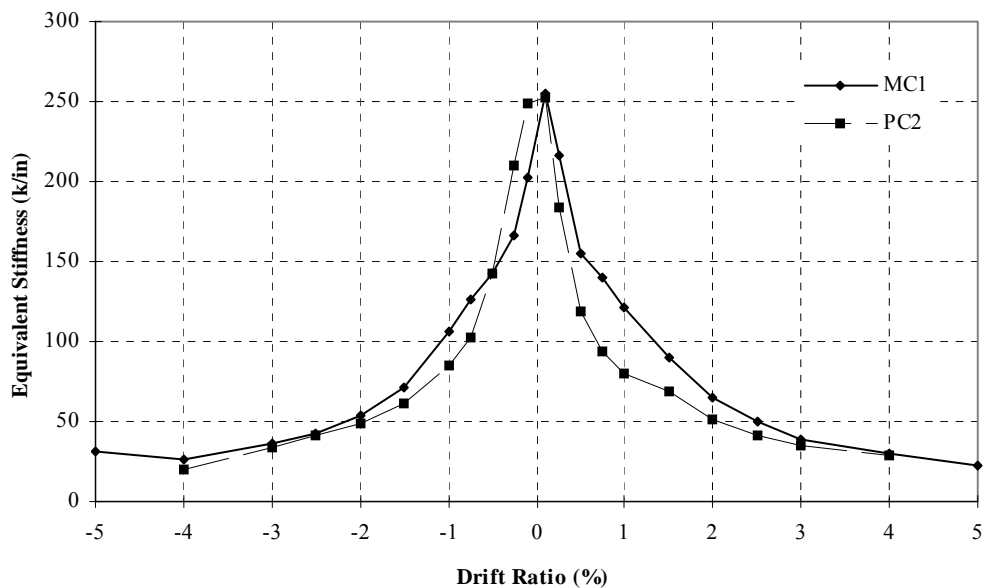


Figure 4.9: Equivalent Stiffness, K_e

Both specimens demonstrated rapid stiffness deterioration. Most of the stiffness degradation occurred through 1.0 percent drift ratio. In subsequent cycles, further equivalent stiffness deterioration occurred primarily due to concrete spalling and increased residual drifts.

In general, Specimen MC1 exhibited higher equivalent stiffness than Specimen PC2, except at negative drift ratios beneath 0.5 percent. As drift ratio increased beyond 1.5 percent, differences between equivalent stiffness values decreased.

4.5.2.2 Peak-to-Peak Stiffness

Figure 4.10 shows the peak-to-peak stiffness plotted versus story drift ratio. In addition, Figure 4.11 provides a comparison between peak-to-peak stiffness and equivalent stiffness for Specimens MC1 and PC2.

The values used to construct Figure 4.10 were obtained from the first cycle at each drift ratio. Once again, these plots demonstrate rapid stiffness deterioration during load cycles to approximately 1.0 percent or smaller drift ratio. Specimen PC2 demonstrated greater losses during the early cycles. Bond deterioration, which occurred in Specimen PC2, did not appear to significantly affect overall peak-to-peak stiffness degradation.

The comparison of peak-to-peak stiffness and equivalent stiffness illustrated in Figure 4.11 indicates that peak-to-peak and equivalent stiffness are approximately the same for Specimen MC1 throughout most of the testing program. Peak-to-peak stiffness was generally greater than equivalent stiffness for

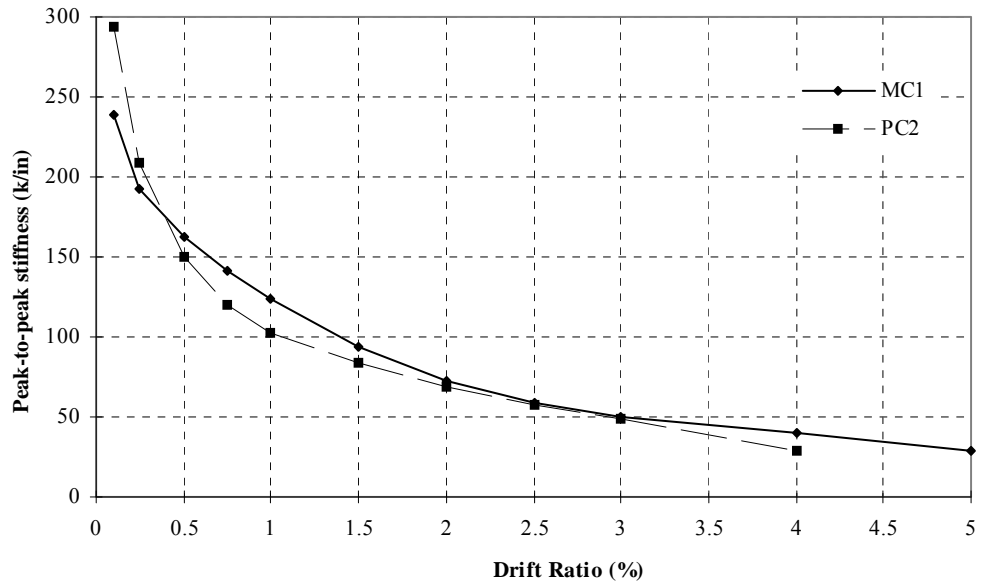


Figure 4.10: Peak-to-peak Stiffness, K_p

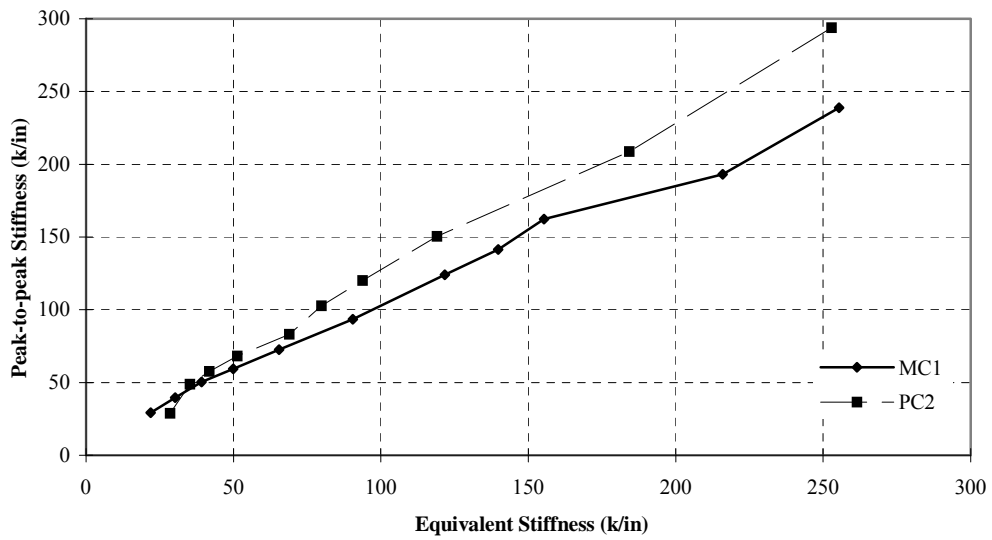


Figure 4.11: Comparison between Equivalent and Peak-to-Peak Stiffnesses

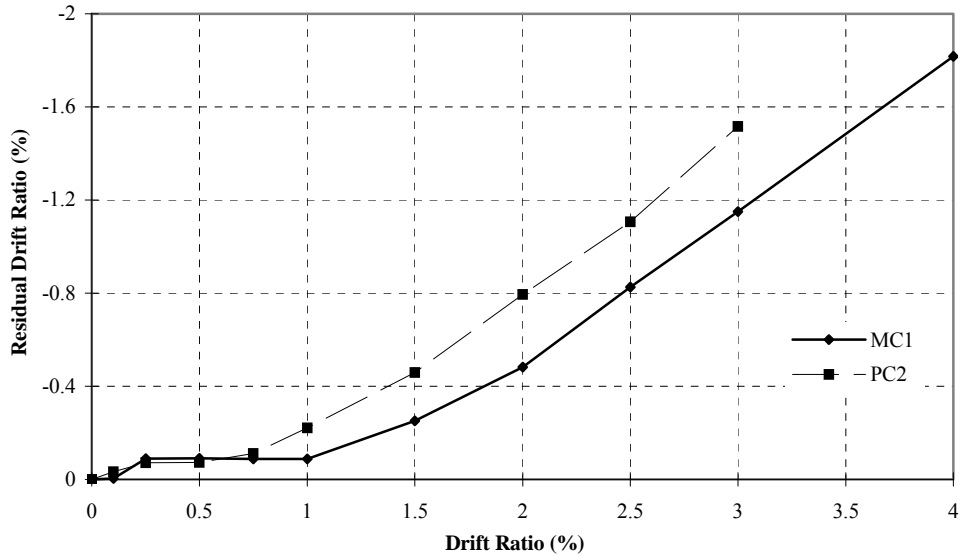


Figure 4.12: Residual Drift Ratios

Specimen PC2. This reflects pinching in the hysteresis loops that resulted from slip of bars in the splice devices in Specimen PC2.

4.6 COMPARISON OF RESIDUAL DEFORMATIONS

The residual drift ratios for Specimens MC1 and PC2 are shown in Figure 4.12. The residual drift was investigated to study the ability of the tested connections to return to their undeformed positions following loading into the inelastic response range. Figure 4.12 presents residual drift data (at zero load) following execution of the last loading cycle at each drift ratio.

Both specimens exhibited very small residual drifts through 0.75 percent drift ratio. Specimen MC1 had well-distributed flexural cracks near the bottom of the column. The maximum widths of most cracks were quite small (less than 0.01

in.). Up through a drift ratio of 3.0 percent, the residual drift of Specimen MC1 remained below 40 percent of the maximum applied drift ratio. However, Specimen PC2 experienced relatively large residual drifts beginning at 1.0 percent. At 1.0 percent drift ratio, the residual drift was approximately one third the maximum applied drift. The crack at the splice base in Specimen PC2 contributed significantly to the residual drift. Slip of the spliced bars was not completely recovered due to frictional resistance within the splice.

From 1.0 to 3.0 percent drift ratio, both specimens experienced approximately the same increase in residual drift ratios. Even though the crack width at the column-base interface continued to increase, residual drifts for Specimen PC2 did not increase at a higher rate than for Specimen MC1, suggesting bar yielding, not bar slip, was responsible for the increase in crack width.

4.7 INTERNAL BEHAVIOR OF SPECIMENS

Strain gauges were installed on selected column reinforcing bars and splice sleeves (see Figs. 2.18 and 2.19). Six strain gauges were attached on the longitudinal column reinforcing bars for all specimens. For Specimens PC1 and PC2, an additional six pairs of strain gauges were attached on selected splice sleeves.

Specimens MC1 and PC2 experienced drift ratios of 4.0 percent or more. Therefore, large strains were expected in the column longitudinal reinforcement. However, few of the strain gauges remained effective at this stage. Data that

appeared to be reliable and most representative of specimen behavior is presented and discussed in this section.

4.7.1 Strain History of a Column Reinforcing Bar in Specimen MC1

Figure 4.13 shows the strain history for a column longitudinal reinforcing bar in Specimen MC1. The strain gauge was installed at the interface of the column and base elements, and was located on the column face that first experienced compression.

As shown in Figure 4.13, strains increased as drift ratio increased, and reached the yield strain at 1.0 percent drift ratio. Up to yield, the maximum positive/tensile strain for each cycle was almost double the corresponding negative/compressive strain.

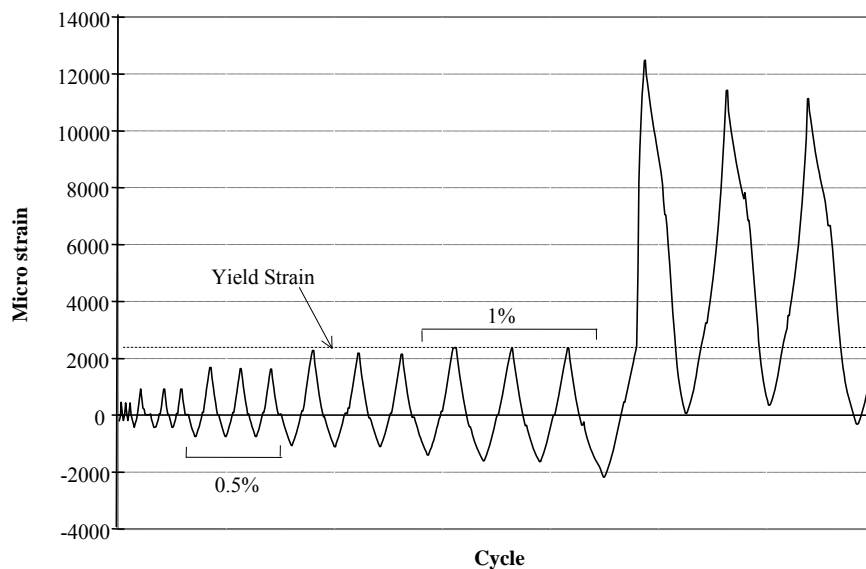


Figure 4.13: Strain History of Column Reinforcing Bar in Specimen MC1

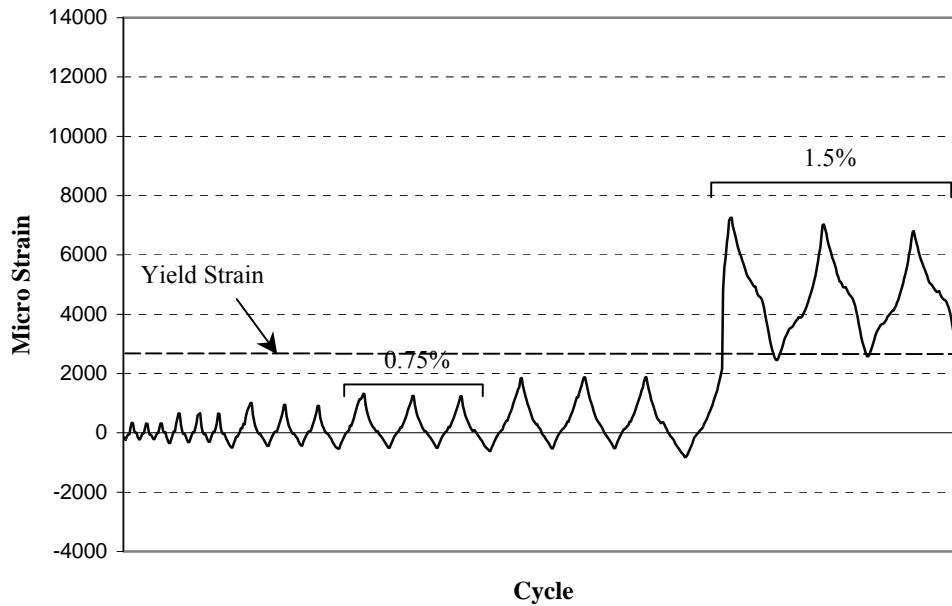


Figure 4.14: Strain History of Column Reinforcing Bar in Specimen PC2

4.7.2 Strain History of Column Reinforcing Bar and Splice Sleeve in Specimen PC2

Figure 4.14 shows the strain history for a spliced bar that extended from the base element. The data for Figure 4.14 were obtained from a strain gauge at the same location as for Specimen MC1.

All column longitudinal reinforcing bars, except one, reached yield at 1.5 percent drift ratio. One corner bar reached yield at the interface at 0.75 drift ratio. Compared to the strain measurements from Specimen MC1, negative/compressive strains in PC2 remained relatively small until 1.0 percent drift ratio. Two reasons account for this difference. First, during unloading, the splices behaved as compression reinforcement at the interface. Therefore, by sharing the

compression force, the splices reduced stresses in the compressed bars. Second, due to slip of the spliced bars during previous loading cycles, only a small compression force was required to cause the bars to slip back toward their original position.

Figure 4.15 shows the strain history for a splice sleeve in Specimen PC2. The splice was designed to remain elastic throughout the test. The chemical bond between the splice sleeve and concrete outside the splice sleeve was ignored. Furthermore, the chemical bond between the splice and cementitious grout was also ignored.

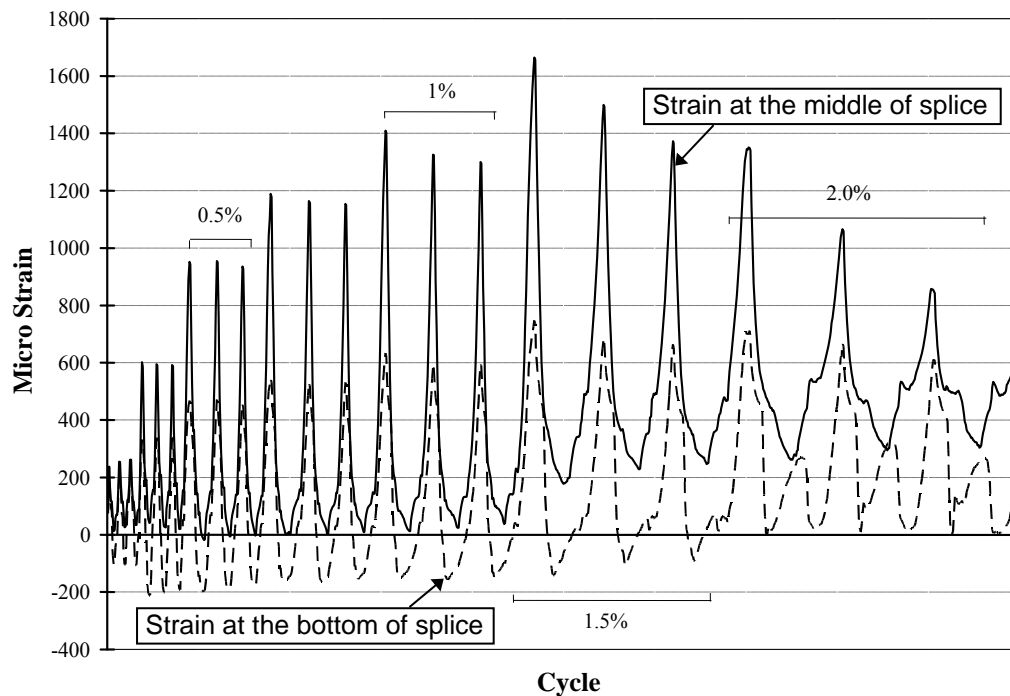


Figure 4.15: Strain History for Splice Sleeve

Two plots are presented in Figure 4.15. One represents data from a strain gauge attached near the lower end of a splice sleeve, and the other represents data from a gauge attached at mid-height of the same splice sleeve.

As shown in Figure 4.15, strains at mid-height of the splice sleeve were approximately twice the strains measured near the lower end. At the lower end, the strain increase corresponding with increase in drift ratio was also relatively small. The strain history at mid-height of the splice shows that the highest strain was reached during the first cycle at each drift level and decreased during the following cycles. This implies that during the first cycle at each drift level, force in the spliced bar surpassed the previous maximum force level. During the following cycles, bond resistance was reduced due to damage incurred during the first cycle. This contrasts the strain data shown in Figure 4.14, which remains constant during cycles to the same drift ratio. Strain data from mid-height of the splice exhibited no signs of compression, even during early stages of loading. Also, strains measured at the lower end of the splice sleeve remained positive after 1.5 percent drift ratio. This implies that the crack opening at the column end did not fully close when the loading direction was reversed because of frictional resistance to closing and concrete debris inside the crack. Measured strains in the splice sleeve decreased when the spliced bars reached yield.

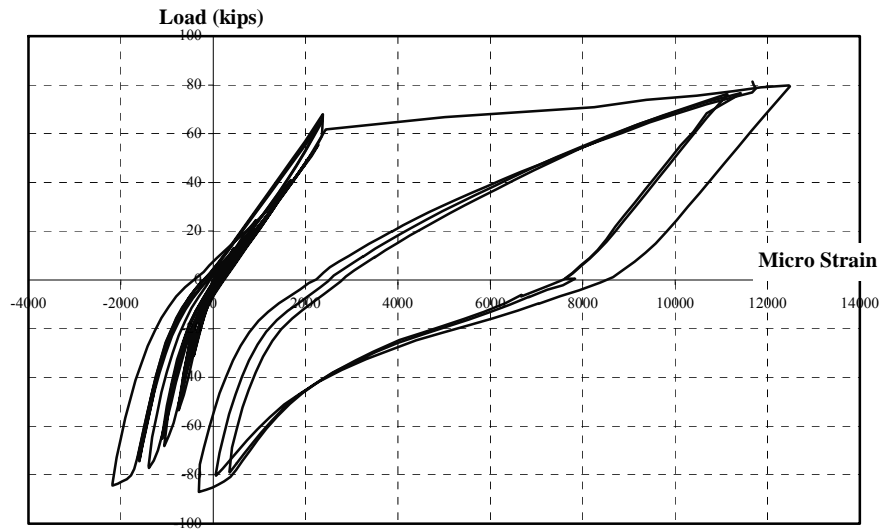


Figure 4.16: Load-Strain Plot of Column Reinforcing Bar in Specimen MC1

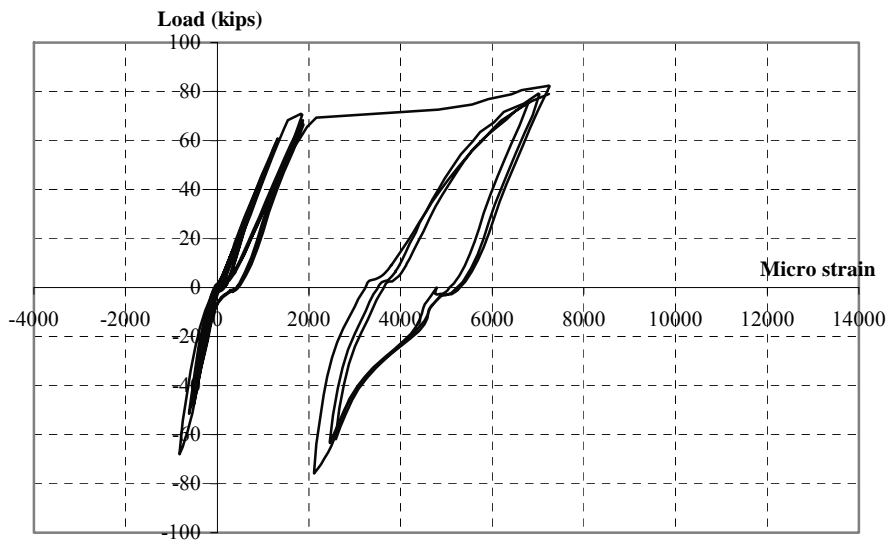


Figure 4.17: Load-Strain Plot of Column Reinforcing Bar in Specimen PC2

4.7.3 Load-Strain Curves for Column Reinforcing Bars

The load-strain plots for column longitudinal reinforcing bars in Specimens MC1 and PC2 are shown in Figures 4.16 and 4.17.

Both plots are drawn for response through the first cycle of 2.0 percent drift ratio. Data beyond 2.0 percent drift ratio are not shown because strain gauge readings were erratic and deemed unreliable. Overall shapes of the load-strain responses from both specimens are very similar.

As shown in Figure 4.16, yielding of the column reinforcing bars in Specimen MC1 occurred during the 1.5 percent drift ratio cycles. The peak load at this drift ratio was 84.4 kips. After yielding, peak loads in both loading directions were very similar.

The load-strain plot for a column longitudinal reinforcing bar in Specimen PC2 is shown in Figure 4.17. Yielding of column longitudinal reinforcing bars occurred during 1.5 percent drift ratio cycles. The peak load was 70.9 kips which was less than the peak load for Specimen MC1 at the same drift ratio. After yielding, however, both specimens reached more than 80 kips. As mentioned in Section 4.7.2, compression strains in the reinforcement remained small before yielding occurred in Specimen PC2. Beyond yield, the column longitudinal reinforcing bars experienced a smaller strain range than Specimen MC1.

CHAPTER 5

CONCLUSIONS AND RECOMMENDATIONS

5.1 INTRODUCTION

Most precast members are produced in fabrication plants and are shipped to the construction site. Connections between precast members are usually completed on site. One of the primary objectives of this study was to examine the behavior of a grout-filled pipe sleeve developed to splice longitudinal reinforcement in seismic-resistant precast concrete columns.

Splicing of column longitudinal reinforcement immediately above the floor level is generally not acceptable in cast-in-place construction, but is desirable in precast construction. Although frame design is generally based on capacity design techniques utilizing a strong column-weak beam design approach, precast column splices immediately above the floor levels must have sufficient strength and toughness to withstand unintended levels of inelastic deformation.

In order to evaluate the strength and deformation characteristics of the splice sleeve, two precast specimens and one cast-in-place control specimen were fabricated. Each precast column was connected to reinforcement extending from a strong base element (representing the beam element that would intersect the column immediately below the splice).

5.2 CONCLUSIONS AND RECOMMENDATIONS

Based on the experimental study, the following conclusions and recommendations are made:

Overall load-deflection response for Specimens PC2 and MC1 was comparable through 0.5 percent drift ratio. Stiffness of Specimens PC2 and MC1 was similar through 0.5 percent drift ratio. At higher drifts, Specimen PC2 exhibited as much as 50 percent more flexibility due to slip of bars in the splice sleeves.

The failure observed for Specimens PC2 and MC1 was quite different; Specimen PC2 failed at 4.0 percent drift ratio due to deterioration of the longitudinal bar splice, while Specimen MC1 failed due to concrete crushing at 5.0 percent drift ratio. Maximum load sustained by Specimens PC2 and MC1 was 92 and 94 kips, respectively. Although response of the well-behaved precast connection (Specimen PC2) and monolithic connection was not identical, test results indicate that the precast connection should provide sufficient strength and toughness when capacity-design techniques are used to proportion members and connections in the vicinity of beam-column connections.

Performance of splice sleeves is heavily influenced by the quality of grout material and grout placement in the splice sleeve. Specimen PC1 performed poorly during testing, reaching a maximum applied load of only 52.5 kips at 2.0 percent drift ratio. Poor performance was related to incomplete grouting of the splice sleeve. Incomplete grouting was caused by segregation of the commercial grout material used in the splice sleeve, by the top grout port location, and by

insufficient clearance between the reinforcing bar and inside of the splice sleeve. A standard cement grout with expansive agent, not the sanded grout used in PC1, and a revised splice sleeve detail (described in Section 4.2) was used for Specimen PC2. The performance of Specimen PC1 underscores the importance of the splice sleeve behavior, which is a function of the details used in the splice sleeve, the quality of the grout, and the grout placement procedure.

The splice sleeve length, which was based on recommendations from research performed by Einea et. al.[4], was satisfactory for the No. 8 bar used. The tests reported by Einea et. al. utilized No. 7 bars, so extrapolation of their recommendations to significantly different bar sizes should be confirmed with additional tests.

Tolerance associated with the splice sleeve connection was nominally ± 0.25 inches. Placement of reinforcement and splice sleeves in precast members must be carefully controlled to accommodate this tolerance.

5.3 ADDITIONAL RESEARCH

The experimental study reported here satisfied the intended research objectives. However, some areas should be investigated further.

The splice sleeve device was used immediately above a heavily reinforced base beam that was secured to the strong structural testing floor. Verification of the performance of the column splice device in an actual precast beam-column connection is desirable.

The splice sleeve device has only been used to splice No. 7 and 8 bars. Larger bar sizes, more representative of actual column longitudinal bar sizes, and higher-strength Grade 75 bars should also be investigated.

Behavior of the precast connection region incorporating the splice sleeve device would likely be different if a representative level of axial load were applied to the column. One or more tests involving different column axial load levels should be carried out.

Splice sleeves utilized in this study were applied to column longitudinal reinforcing bars. Application of the splice sleeves for beam reinforcing bars may require different grout port details.

Appendix

Glossary

| Symbol | Description |
|-----------------------|---|
| d | Nominal diameter of a bar (in.) |
| f'_c | Specified compressive strength of concrete (psi) |
| f'_{cg} | Specified compressive strength of grout (psi) |
| f_u | Ultimate strength of reinforcement (ksi) |
| f_y | Specified yield strength of nonprestressed reinforcement (ksi) |
| H | Column height (in.) |
| H_{eq} | Equivalent viscous damping ratio |
| K_e | Equivalent stiffness (k/in.) |
| K_p | Peak-to-peak stiffness (k/in.) |
| K_{sec} | Secant stiffness (k/in.) |
| L_d | Embedment length of a spliced bar (in.) |
| R | Drift angle (%) |
| U | Average bond stress (psi) |
| P | Applied lateral load (kips) |
| $P_{u,calc}$ or P_u | Calculated ultimate lateral load capacity (kips) |
| $P_{u,exp}$ | Ultimate lateral load capacity measured from an experiment (kips) |
| Δ | Relative displacement (drift) of column (in.) |
| Δ^* | Story drift corresponding to $0.75P_u$ (in.) |
| Δ_u | Maximum measured drift |
| Δ_y | Yield displacement (in.) |

| Symbol | Description |
|--------------|-------------------------------------|
| ϵ_y | Yield strain of reinforcement (ksi) |
| μ | Displacement ductility |

Reference

1. Uniform Building Code, 1991 Edition, International Conference of Building Officials, Whittier, Calif.
2. American Concrete Institute (ACI), Building Code Requirements for Reinforcement Concrete and Commentary – 318-89, Detroit, 1989.
3. ACI Committee 408, “Bond Stress – The State of the Art,” ACI Journal Proceedings, V.63, No.11, Nov. 1966, pp. 1161-1188.
4. Einea, A; Yamane, T; Tadros, M. K., “Grout-Filled Pipe Splices for Precast Concrete Construction,” PCI Journal, V.40, No.1, Jan.-Feb. 1995, pp. 82-93.
5. Wang, C; Salmon, C.G., Reinforced Concrete Design, Fourth Edition, Harper & Row, New York, 1985.
6. Rezansoff, Telvin; Zacaruk, Jim A.; Topping, Rob, “Tensile Lap Splices in Reinforced Concrete Beams under Inelastic Cyclic Loading,” ACI Structural Journal, V.85, No.1, Jan.-Feb. 1988, pp. 46-52.
7. Durrani, Ahmad J.; Wight, James K., “Earthquake Resistance of Reinforced Concrete Interior Connections Including a Floor Slab,” ACI Structural Journal, V.83, No.5, Sep.-Oct. 1987, pp.400-406.
8. Soroushian, Parviz; Choi, Ki-Bong; Park, Gill-Hyun; Aslani, Farhang, “Bond of Deformed Bars to Concrete: Effects of Confinement and Strength of Concrete,” ACI Material Journal, V.88, No.3, May-June 1991, pp. 227-232.

9. Cheok, Geraldine S.; Lew, H. S., "Performance of Precast Concrete Beam-to-Column Connections Subjected to Cyclic Loading," PCI Journal, V.36, No.3, May-June 1991, pp. 56-67.
10. Cheok, Geraldine S.; Lew, H. S., "Model Precast Concrete Beam-to-Column Connections Subjected to Cyclic Loading," PCI Journal, V.38, No.4, July-Aug. 1993, pp. 80-92.

Vita

Yong-mook Kim, son of Kyoung-soo Kim and Young-ja Moon, was born April 21, 1966, in Seoul, South Korea. He graduated with Honors from Dae-sung High School in February, 1984. In March, 1984, he began his college studies at In-ha University. In February, 1992, he graduated with a highest honors from In-ha University with a B.S. degree in Architectural Engineering. During summer in 1993, he entered the Graduate School at The University of Texas at Austin.

Permanent address: 3483-D Lake Austin Blvd.
Austin, TX. 78703

This thesis was typed by the author.